Gastroenterology 2020;158:1433–1449

Diphenylbutylpiperidine Antipsychotic Drugs Inhibit Prolactin Receptor Signaling to Reduce Growth of Pancreatic Ductal Adenocarcinoma in Mice

Prasad Dandawate,[1] Gaurav Kaushik,[2] Chandrayee Ghosh,[1] David Standing,[1] Afreen Asif Ali Sayed,[1] Sonali Choudhury,[1] Dharmalingam Subramaniam,[1] Ann Manzardo,[3] Tuhina Banerjee,[4] Santimukul Santra,[4] Prabhu Ramamoorthy,[1] Merlin Butler,[3] Subhash B. Padhye,[1,5] Joaquina Baranda,[6] Anup Kasi,[6] Weijing Sun,[6] Ossama Tawfik,[7] Domenico Coppola,[8] Mokenge Malafa,[8] Shahid Umar,[2] Michael J. Soares,[7,9,10,11] Subhrajit Saha,[12] Scott J. Weir,[1,13] Animesh Dhar,[1] Roy A. Jensen,[1,7] Sufi Mary Thomas,[1,14] and Shrikant Anant[1,2,5]

[1]Department of Cancer Biology, University of Kansas Medical Center, Kansas City, Kansas; [2]Department of Surgery, University of Kansas Medical Center, Kansas City, Kansas; [3]Department of Psychiatry and Behavioral Sciences, University of Kansas Medical Center, Kansas City, Kansas; [4]Department of Chemistry, Pittsburg State University, Pittsburg, Kansas; [5]Interdisciplinary Science and Technology Research Academy, Abeda Inamdar College, University of Pune, Pune; [6]Department of Internal Medicine, University of Kansas Medical Center, Kansas City, Kansas; [7]Department of Pathology and Laboratory Medicine, University of Kansas Medical Center, Kansas City, Kansas; [8]Department of Gastrointestinal Oncology, H. Lee Moffitt Cancer Center and Research Institute, Tampa, Florida; [9]Department of Obstetrics and Gynecology, University of Kansas Medical Center, Kansas City, Kansas; [10]Department of Pediatrics, University of Kansas Medical Center, Kansas City, Kansas; [11]Center for Perinatal Research, Children's Research Institute, Children's Mercy–Kansas City, Kansas City, Missouri; [12]Department of Radiation Oncology, University of Kansas Medical Center, Kansas City, Kansas; [13]Department of Pharmacology, Toxicology and Therapeutics, University of Kansas Medical Center, Kansas City, Kansas; and [14]Department of Otolaryngology, University of Kansas Medical Center, Kansas City, Kansas

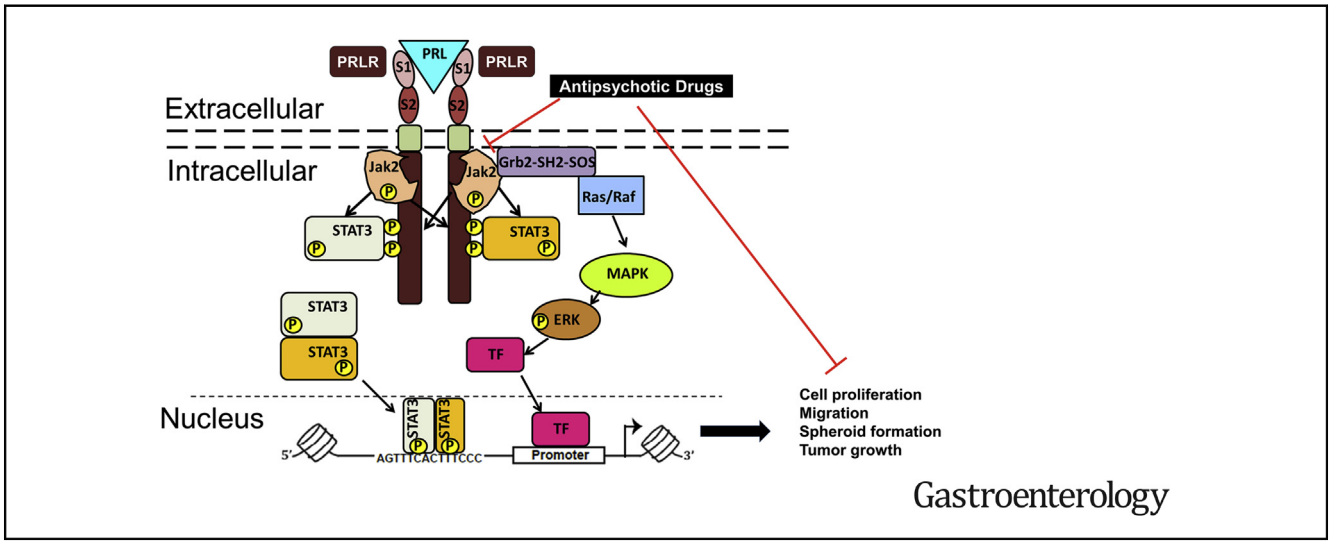

BACKGROUND & AIMS: Prolactin (PRL) signaling is up-regulated in hormone-responsive cancers. The PRL receptor (PRLR) is a class I cytokine receptor that signals via the Janus kinase (JAK)–signal transducer and activator of transcription and mitogen-activated protein kinase pathways to regulate cell proliferation, migration, stem cell features, and apoptosis. Patients with pancreatic ductal adenocarcinoma (PDAC) have high plasma levels of PRL. We investigated whether PRLR signaling contributes to the growth of pancreatic tumors in mice. **METHODS:** We used immunohistochemical analyses to compare levels of PRL and PRLR in multitumor tissue microarrays. We used structure-based virtual screening and fragment-based drug discovery to identify compounds likely to bind PRLR and interfere with its signaling. Human pancreatic cell lines (AsPC-1, BxPC-3, Panc-1, and MiaPaCa-2), with or without knockdown of PRLR (clustered regularly interspaced short palindromic repeats or small hairpin RNA), were incubated with PRL or penfluridol and analyzed in proliferation and spheroid formation. C57BL/6 mice were given injections of UNKC-6141 cells, with or without

knockdown of PRLR, into pancreas, and tumor development was monitored for 4 weeks, with some mice receiving penfluridol treatment for 21 days. Human pancreatic tumor tissues were implanted into interscapular fat pads of NSG mice, and mice were given injections of penfluridol daily for 28 days. Nude mice were given injections of Panc-1 cells, xenograft tumors were grown for 2 weeks, and mice were then given intraperitoneal penfluridol for 35 days. Tumors were collected from mice and analyzed by histology, immunohistochemistry, and immunoblots. **RESULTS:** Levels of PRLR were increased in PDAC compared with nontumor pancreatic tissues. Incubation of pancreatic cell lines with PRL activated signaling via JAK2–signal transducer and activator of transcription 3 and extracellular signal–regulated kinase, as well as formation of pancospheres and cell migration; these activities were not observed in cells with PRLR knockdown. Pancreatic cancer cells with PRLR knockdown formed significantly smaller tumors in mice. We identified several diphenylbutylpiperidine-class antipsychotic drugs as agents that decreased PRL-induced JAK2 signaling; incubation of pancreatic cancer cells with these compounds reduced their proliferation and formation of panco spheres. Injections of 1 of these compounds, penfluridol, slowed the growth of xenograft tumors in the different mouse models, reducing proliferation and inducing autophagy of the tumor cells. **CONCLUSIONS:** Levels of PRLR are increased in PDAC, and exposure to PRL increases proliferation and migration of pancreatic cancer cells. Antipsychotic drugs, such as penfluridol, block PRL signaling in pancreatic cancer cells to reduce their proliferation, induce autophagy, and slow the growth of xenograft tumors in mice. These drugs might be tested in patients with PDAC.

Keywords: Dopamine Receptor; Molecular Modeling; Combination Therapy; Gemcitabine.

WHAT YOU NEED TO KNOW

BACKGROUND AND CONTEXT

Prolactin signaling is upregulated in hormone-responsive cancers, and patients with pancreatic ductal adenocarcinoma (PDAC) have high plasma levels of prolactin. The prolactin receptor (PRLR) signals via the JAK–STAT and MAPK pathways to regulate cell proliferation, migration, stem-cell features, and apoptosis.

NEW FINDINGS

Levels of PRLR are increased in PDAC, and exposure of pancreatic cancer cells to PRL increases their proliferation and migration. Antipsychotic drugs such as penfluridol block PRLR signaling in pancreatic cancer cells and reduced their proliferation, induced autophagy, and slowed growth of xenograft tumors in mice.

LIMITATIONS

This study was performed in cell lines and mice. Studies in humans are needed.

IMPACT

Antipsychotic drugs such as penfluridol block JAK2 signaling in pancreatic cancer cells, slow tumor growth in mice, and might be tested in patients with PDAC.

Prolactin (PRL) signaling has an established role in maintaining pregnancy, mammary gland development, immune regulation, adipocyte control, reproduction, and islet cell differentiation.[1,2] Moreover, the pathway is implicated in multiple endocrine-driven tumors.[3] More recently, the pathway has been observed to play a role in other tumor types, including colon and hepatocellular cancers.[4,5] PRL receptor (PRLR) belongs to the class I cytokine receptor superfamily and lacks intrinsic kinase activity, transducing signals including Janus kinase (JAK)–signal transducer and activator of transcription (STAT) and mitogen-activated protein kinase (MAPK) pathways through kinases that interact with its cytoplasmic tail.[6] The pathway is implicated in the promotion of cell proliferation, migration, stemness, and inhibition of apoptosis,[7] as well as chemoresistance.[8,9] In colon cancers, PRL induces JAK2–STAT3 signaling to affect stemness by up-regulating the Notch pathway.[5]

We now show that PRLR-based signaling is active in pancreatic ductal adenocarcinoma (PDAC). The reason for choosing PDAC is 2-fold: first, patients with PDAC have high plasma levels of PRL[10]; second, PDAC remains a leading cause of cancer-related deaths in the United States.[11] Poor prognosis, drug resistance, and high recurrence rates characterize PDAC after surgery.[12] Here, we show that PRL induces both JAK2–STAT3 and extracellular signal–regulated kinase (ERK) signaling in the cells. PRLR knockdown reduced the signaling and tumor growth in the orthotopic PDAC model, suggesting that PRLR may be an effective therapeutic target. To identify a small-molecule inhibitor, we developed an in silico model for the JAK2-interacting domain and subsequently identified potential interacting diphenylbutylpiperidine (penfluridol, pimozide, fluspirilene) and phenothiazine (promethazine) antipsychotic compounds. Using penfluridol as proof of principle, we show that it is effective in targeting PRLR signaling and suppressing tumor growth in the orthotopic PDAC model. Because penfluridol was initially identified as a dopamine receptor D2 (DRD2) antagonist, we also determined whether its effect also occurs through DRD2. Although DRD2 expression is also induced in PDAC, the penfluridol effect on PDAC cells was not affected by DRD2 knockdown. This suggests that the penfluridol effect occurs through suppression of PRLR signaling.

Abbreviations used in this paper: **AKT, protein kinase B; CRISPR, clustered regularly interspaced short palindromic repeats; DMEM, Dulbecco's modified Eagle medium; DRD2, dopamine receptor D2; ERK, extracellular signal–regulated kinase; FBS, fetal bovine serum; JAK, Janus kinase; MAPK, mitogen-activated protein kinase; mRNA, messenger RNA; PDAC, pancreatic ductal adenocarcinoma; PDX, patient-derived xenograft; PRL, prolactin; PRLR, prolactin receptor; shRNA, short hairpin RNA; SPR, surface plasmon resonance; STAT, signal transducer and activator of transcription; TCGA, The Cancer Genome Atlas; TMA, tumor microarray.**

Most current article

0016-5085/$36.00
https://doi.org/10.1053/j.gastro.2019.11.279

Materials and Methods

Please refer to the Supplementary Materials for detailed additional methods.

Cells and Culture Condition

Human PDAC cell lines AsPC-1, BxPC-3, Panc-1, and MiaPaCa-2 (all obtained from American Type Culture Collection (Manassas, VA), Panc 2.15, Panc 3.014, Panc 5.04, Panc 8.13, and Panc 10.05 were gifts from *Johns Hopkins* University (Baltimore, MD). The UNKC-6141 cell line was a gift from Dr Surinder Batra. The cell lines were grown in RPMI 1640 or Dulbecco's modified Eagle medium (DMEM) with 4.5 g/L glucose, L-glutamine, and sodium pyruvate (Corning, Tewksbury, MA) containing 10% heat-inactivated fetal bovine serum (FBS) (Sigma-Aldrich, St. Louis, MO) and 1% antibiotic-antimycotic solution (Corning) at 37°C in a humidified atmosphere of 5% CO_2. HPNE cells were kindly provided by Dr

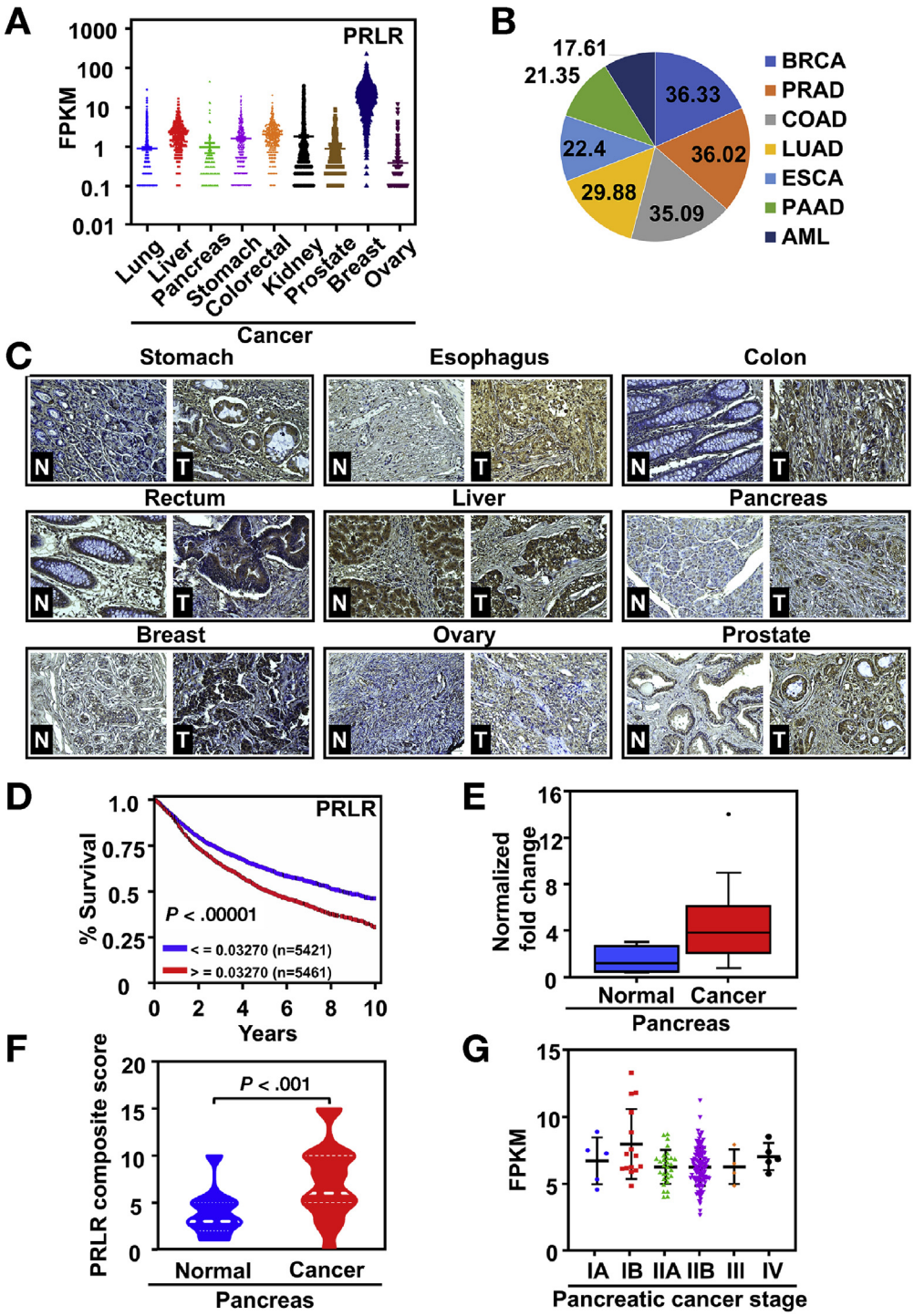

Figure 1. PRLR is up-regulated in PDAC. (*A*) PRLR mRNA levels are high in multiple cancers in the TCGA database. (*B*) The PRLR pathway gene set, analyzed by GeneAnalytics, shows that PRLR pathway genes are up-regulated in various cancer types: breast (BRCA), prostate adenocarcinoma (PRAD), colon adenocarcinoma (COAD), lung adenocarcinoma (LUAD), esophageal carcinoma (ESCA), pancreatic adenocarcinoma (PAAD), and acute myeloid leukemia (AML). (*C*) Immunohistochemistry of a multiple-organ TMA shows that PRLR is differentially up-regulated in several cancers (T) when compared with normal tissue (N). (*D*) Kaplan–Meier plot shows that high PRLR gene copy number correlates with low survival in patients with cancer ($P < .00001$). The TCGA pan-cancer (PanCan) cohort. (*E*) Real-time polymerase chain reaction analyses shows that PRLR expression is higher in PDAC compared with normal samples ($P < .05$). (*F*) Composite score of PDAC TMA shows significantly higher expression of PRLR in tumors compared with normal pancreas ($P < .001$). (*G*) PRLR mRNA is up-regulated early in PDAC progression, generated from the TCGA data sets. FPKM, fragments Per Kilobase of transcript per Million mapped reads.

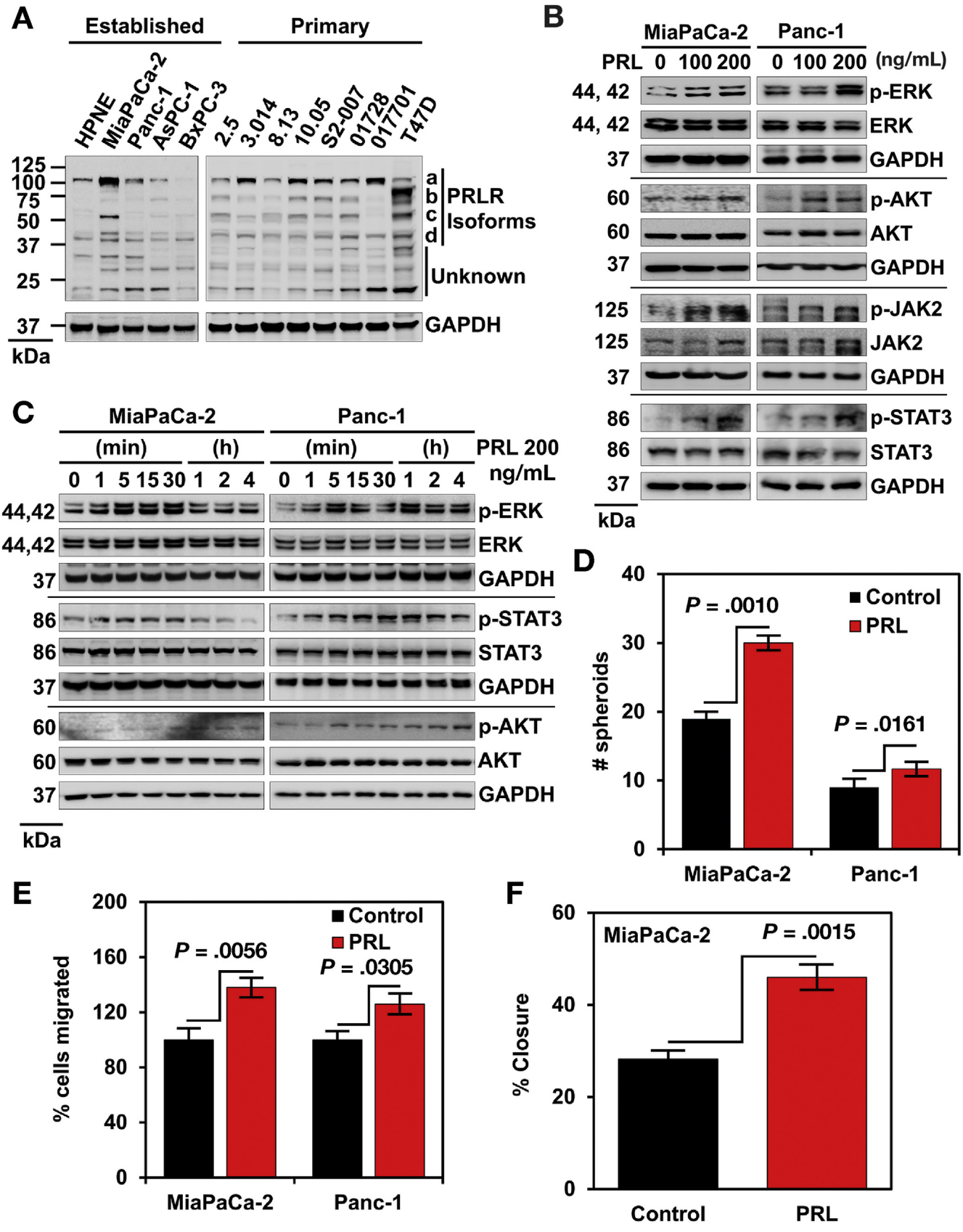

Anirban Maitra and were grown in DMEM with 4.5 g/L glucose, L-glutamine, and sodium pyruvate (Corning) with 5% FBS, 10 ng/mL bFGF (basic fibroblast growth factor), and 50 μg/mL gentamycin. All the cell lines used in this study were within 20 passages after receipt or resuscitation (approximately 3 months of noncontinuous culturing).

Proliferation and Apoptosis Assays

Pancreatic cancer cells were plated in 96-well plates, allowed to grow for 24 hours, and treated with increasing doses of respective compounds. Cell proliferation was measured by enzymatic hexosaminidase assay, as described previously.[1] For apoptosis, the Apo-one Homogeneous Caspase-3/7 Assay kit was used to calculate caspase 3/7 activity (Promega, Madison, WI).

Clonogenicity Assay

Briefly, 350 viable pancreatic cancer cells per well were seeded in 6-well dishes and treated with penfluridol in 10% FBS containing RPMI1640/DMEM for 48 hours; then medium with or without compound was removed, and the cells were incubated for an additional 10 days in fresh complete medium to form colonies. The colonies were fixed with formalin and stained with crystal violet.

Animal Studies

Pancreatic Ductal Adenocarcinoma Orthotopic Model in Mice. Five-week-old male C57BL/6 mice purchased from The Jackson Laboratory (Sacramento, CA) were maintained with standard mouse chow ad libidum and used in protocols approved by the University's Animal Studies Committee. Animals were injected with 1×10^6 UNKC-6141,[13] empty vector, and UNKC-6141 KD cells in the pancreas and allowed to grow for 4 weeks. In another experiment, 1 week after implantation, penfluridol (5 mg/kg body weight) was administered intraperitoneally daily for 21 days. At the end of treatment, the animals were euthanized, and the tumors were removed, weighed, and used for histology (H&E), immunohistochemistry, and Western blot studies.

Pancreatic Ductal Adenocarcinoma Patient-Derived Xenograft Model. For the patient-derived xenograft (PDX) model, we obtained PDX-carrying NSG mice from The Jackson Laboratory (Sacramento, CA) (TM01212). The cryopreserved tumor tissue obtained from patients with pancreatic cancer was cut into small pieces. The animals were anesthetized, and then the tissue was implanted subcutaneously into the interscapular fat pad by making a shallow incision in the dorsal region. Once tumors were established, we started to treat the mice with penfluridol 5 mg/kg intraperitoneally for 28 days. Tumor size was measured weekly. At the end of treatment, the animals were euthanized, and the tumors were removed and weighed.

Panc-1 Xenograft Tumors in Mice. Five-week-old male athymic nude mice were procured from Charles River Laboratory and maintained with water and standard mouse chow ad libidum. All study protocols were approved by the University's Animal Studies Committee. In brief, 1×10^6 Panc-1 cells were injected in the left and right flank of the mice and allowed to grow a xenograft for a week. One week after injection, a palpable tumor was observed. Subsequently, penfluridol (5 mg/kg) was administered intraperitoneally for 35 days. Tumor volumes were measured weekly. At the end of treatment, the animals were euthanized, and the tumors were removed, weighed, and used for histology (H&E), immunohistochemistry, and Western blot studies.

Statistical Analysis

All values are expressed as the mean ± standard error of the mean. Data were analyzed with an unpaired 2-tailed *t* test. A *P* value of less than .05 was considered statistically significant.

Results

Prolactin Receptor Is Up-regulated in Pancreatic Ductal Adenocarcinoma and Other Cancers

To investigate the role of PRLR in cancers, we first assessed expression in normal tissues and cancers using RNA-sequencing data generated by the Genotype-Tissue Expression project. PRLR messenger RNA (mRNA) expression is low in the normal pancreas and prostate compared with other organs (Supplementary Figure 1*A*). However, PRLR mRNA levels are high in all cancers (Figure 1*A*). We next analyzed PRLR gene expression with GeneAnalytics (LifeMap Sciences, Inc., Alameda, CA), using a set of PRL-signaling genes (Supplementary Figure 1*B*).[14] There were 142 PRL-signaling genes that matched to 919 entities, which represented 381 cell types, 81 anatomic compartments, 35 organs/tissues, and 422 hits from high-throughput compound screening studies. Cerebrum and pancreatic islets exhibited the highest match scores, ranging from 3.9 to 3.4 in normal tissues, and breast cancer (score, 36.33) and PDAC (score, 21.35) were the highest among cancers (Supplementary Figures 1*C* and *D* and Figure 1*B*). To confirm PRLR increase in cancers, we

Figure 2. PRLR signals through JAK2–STAT3–ERK–AKT phosphorylation. (*A*) Western blot analysis shows that PRLR is up-regulated in PDAC cell lines. Breast cancer cell line T47D is used as positive control. Different isoforms of PRLR (110 [a], 80 [b], 50 [c], and 40 [d] kDa) are shown. (*B*) Western blot analyses of PDAC cell lysates after treatment with 100 and 200 ng/mL PRL for 30 minutes in serum free media shows increased phosphorylation of ERK1/2, AKT, JAK2, and STAT3 proteins. (*C*) Western blot of lysates after treatment of PDAC cells with 200 ng/mL PRL for up to 4 hours in serum-free media shows a time-dependent increase in ERK1/2 and STAT3 phosphorylation. (*D*) PRL affects pancosphere formation. PDAC cells were grown in ultra-low-binding plates and treated with increasing doses of PRL. There were increased spheroid numbers after PRL (200 ng/mL) treatment in MiaPaCa-2 ($P = .0010$) and Panc-1 ($P = .0161$) cells. (*E*) PRL (200 ng/mL) treatment induces cell migration over a period of 12 hours in MiaPaCa-2 ($P = .0056$) and Panc-1 ($P = .0305$) cells. (*F*) PRL (200 ng/mL) affects migration in scratch plate assay ($P = .0015$). GAPDH, glyceraldehyde-3-phosphate dehydrogenase; min, minutes.

performed immunohistochemical analyses of multitumor tissue microarrays. We observed up-regulation of PRLR expression in various cancers, including the pancreas (Figure 1*C* and Supplementary Figure 1*E*). More importantly, the protein is also intracellular, raising the question of its role inside the cell. Moreover, an increase in

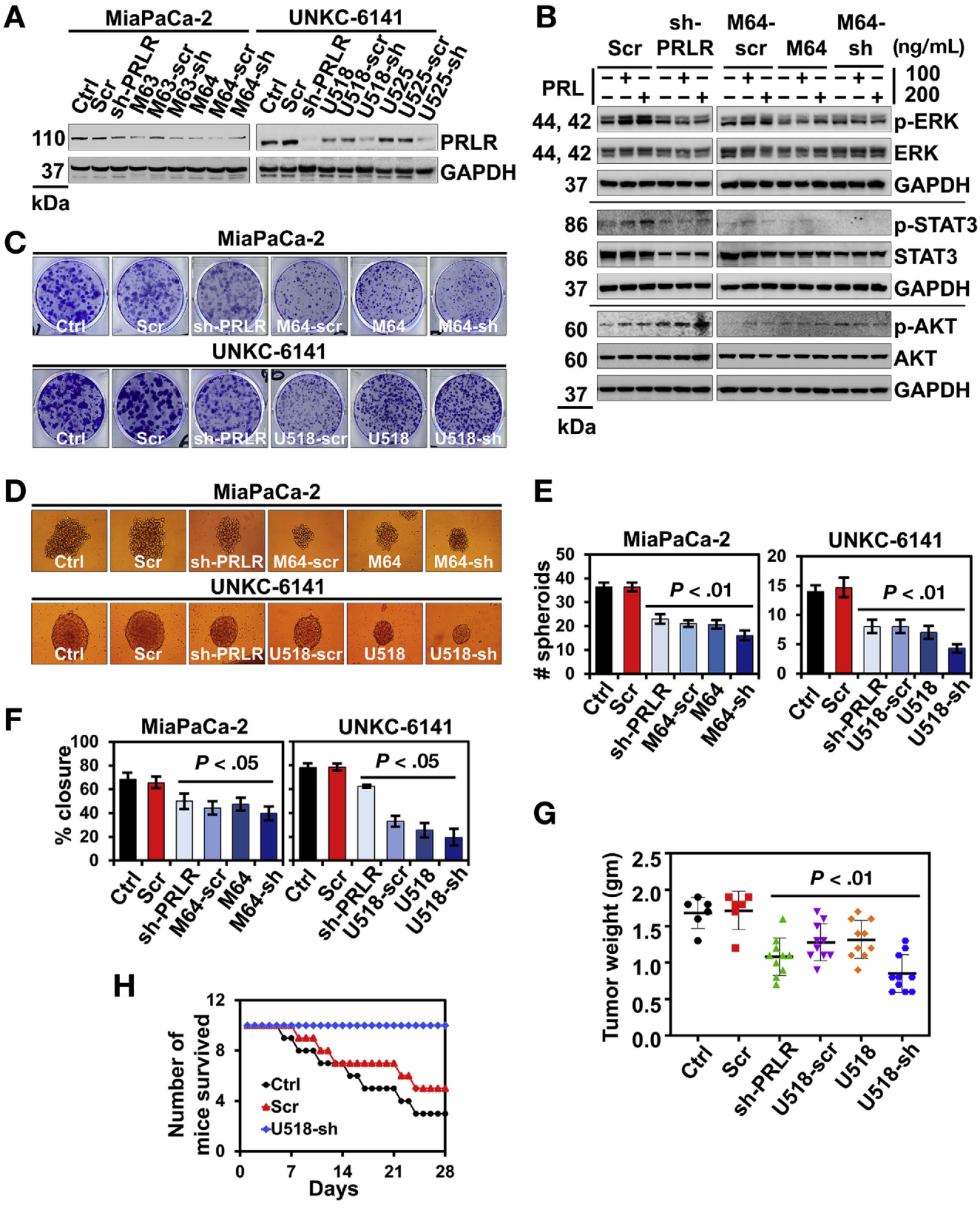

gene copy number correlated with poor survival in cancer patients in the PanCan database of The Cancer Genome Atlas (TCGA) ($P < .0001$) (Figure 1*D*). These data suggest that PRLR is up-regulated in multiple tumor types, especially PDAC, a cancer with high mortality and poor 5-year survival rates.[15]

In normal pancreatic tissue, PRLR expression is low and restricted to islets (Supplementary Figure 1*A* and *F*). In contrast, PRLR mRNA levels were significantly higher in cancer tissues compared with normal samples (Figure 1*E*), which was confirmed by immunohistochemistry (Figure 1*F* and Supplementary Figure 1*F–K*). Interrogation of the TCGA database also showed higher levels of PRLR mRNA in pancreatic cancers (Supplementary Figure 1*L*). The high level of PRLR expression was observed early in the tumorigenesis process (Supplementary Figure 1*G*). We also assessed PRL levels. In normal tissues, PRL mRNA expression is observed in breast, ovary, pancreas, and prostate (Supplementary Figure 1*M*). However, the transcript is expressed in multiple cancers (Supplementary Figure 1*N*). In addition, Kaplan–Meier analyses of data from the TCGA PanCan database showed significantly lower survival ($P < .0001$) in patients with higher PRL copy number (Supplementary Figure 1*O*). Mining of previously reported microarray data also suggested significantly higher PRL levels in primary PDACs (n = 145, $P = .0042$) compared with normal pancreatic tissue (n = 46) (Supplementary Figure 1*P*). In normal pancreas, PRL expression is seen in the β cells, w surrounding acinar cells show lower expression. However, PRL expression is up-regulated in PDAC tissues, irrespective of cancer stage (Supplementary Figure 1*Q*). Similarly, we also observed higher PRL protein levels in established cell lines and primary patient-derived PDAC cells compared with immortalized pancreatic ductal epithelial cell line HPNE (Supplementary Figure 1*R*).

Dopamine plays a predominant role in regulation of PRL release,[16] and DRD2 is present in PDAC tissues.[17] To understand the role of DRD2, we first analyzed RNA-sequencing data generated by the Genotype-Tissue Expression project. DRD2 mRNA expression is low in the normal tissues, but it is increased across several cancers (Supplementary Figure 1*S* and *T*). The TCGA data set also showed DRD2 overexpression in patients with PDAC ($P < .01$) (Supplementary Figure 1*U*). In addition, Kaplan–Meier analyses of data from the TCGA PanCan data set showed a somewhat lower survival ($P = .0912$) in patients with higher DRD2 expression (Supplementary Figure 1*V*). To confirm the up-regulation of DRD2 in PDAC, we used the same tumor microarray (TMA) as that used to probe for PRLR. In normal tissue, DRD2 levels were high in islet cells (Supplementary Figure 1*W*). However, there was a significant increase in DRD2 expression in PDAC tissues ($P < .01$) (Supplementary Figure 1*W–Y*).

Prolactin Receptor Signals Through Janus Kinase 2–Signal Transducer and Activator of Transcription 3–Extracellular Signal–Regulated Kinase–Protein Kinase B Phosphorylation

Alternative spliced transcript variants of PRLR have been identified that encode different membrane-bound and soluble isoforms.[18] Of these, the full-length 110-kDa protein[19] is expressed at higher levels in PDAC cells than HPNE cells (Figure 2*A*). PRLR protein is present in both the nucleus and cytoplasm in PDAC cells (Supplementary Figure 2*A*). On binding to PRLR, PRL activates the JAK2–STAT3 and JAK2–MAPK/protein kinase B (AKT) signaling pathways.[6,20,21] In PDAC cells, recombinant PRL increased phosphorylation of JAK2, STAT3, ERK, and AKT in both a dose- and time-dependent manner (Figure 2*B* and *C*).

Previous reports suggest that PRL induces proliferation, migration, and spheroid formation.[5,22,23] Although PRL did not affect cell proliferation (Supplementary Figure 2*A*), it did increase the size and number of panco spheroids in a dose-dependent manner (Figure 2*D* and Supplementary Figure 2*C*). The significance of this finding is that tumor-derived spheroids are uniquely enriched for cells with stem cell–related characteristics.[24] Another important point about cells with higher spheroid-forming capacity is that they are also highly motile.[25] Our data show that PRL induces cell migration, as assessed by a Transwell chamber (Millipore Sigma, Burlington, MA) (Figure 2*E* and Supplementary Figure 2*D*) and scratch closure assays (Figure 2*F* and Supplementary Figure 2*E*).

Prolactin Receptor Knockdown Affects Pancreatic Ductal Adenocarcinoma Growth

To show that PRLR signaling is important for PDAC growth, we sought to knock out the gene using the clustered regularly interspaced short palindromic

Figure 3. PRLR knockdown affects PDAC growth. (*A*) Western blot shows PRLR knockdown after CRISPR/Cas9 and shRNA in MiaPaCa-2 (human PDAC) and UNKC-6141 (mouse PDAC) cells. M63 and M64, and U518 and U525, are CRISPR/Cas9-knockdown clones of MiaPaca-2 and UNKC-6141, respectively. These cells were further subjected to PRLR-specific (sh) and scrambled (Scr) shRNAs. (*B*) Western blot analyses of MiaPaCa-2 cells treated with PRL (200 ng/mL, 30 minutes) shows no induction in phosphorylation of STAT3, AKT, and ERK1/2, in PRLR-knockdown cells. (*C*) Clonogenicity assay. PRLR-knockdown MiaPaCa-2 and UNKC-6141 cells show comparatively lower colony-forming ability than their respective control cells ($P < .01$). (*D*) PRLR knockdown significantly reduced pancosphere formation. (*E*) PRLR knockdown cells showed reduced spheroid size and number compared with their respective control cells ($P < .01$). (*F*) PRLR knockdown reduced migration ability in scratch plate assay ($P < .05$). (*G*) Mice carrying UNKC-6141 tumors in the pancreas expressing PRLR had significantly lower weight compared with those lacking PRLR (U518, n = 10) ($P < .01$). (*H*) Kaplan–Meier plot shows that animals (n = 10) harboring PRLR knockdown PDAC cells (U518-sh) had a significantly higher survival rate compared with controls ($P < .01$). Ctrl, control; GAPDH, glyceraldehyde-3-phosphate dehydrogenase; gm, gram.

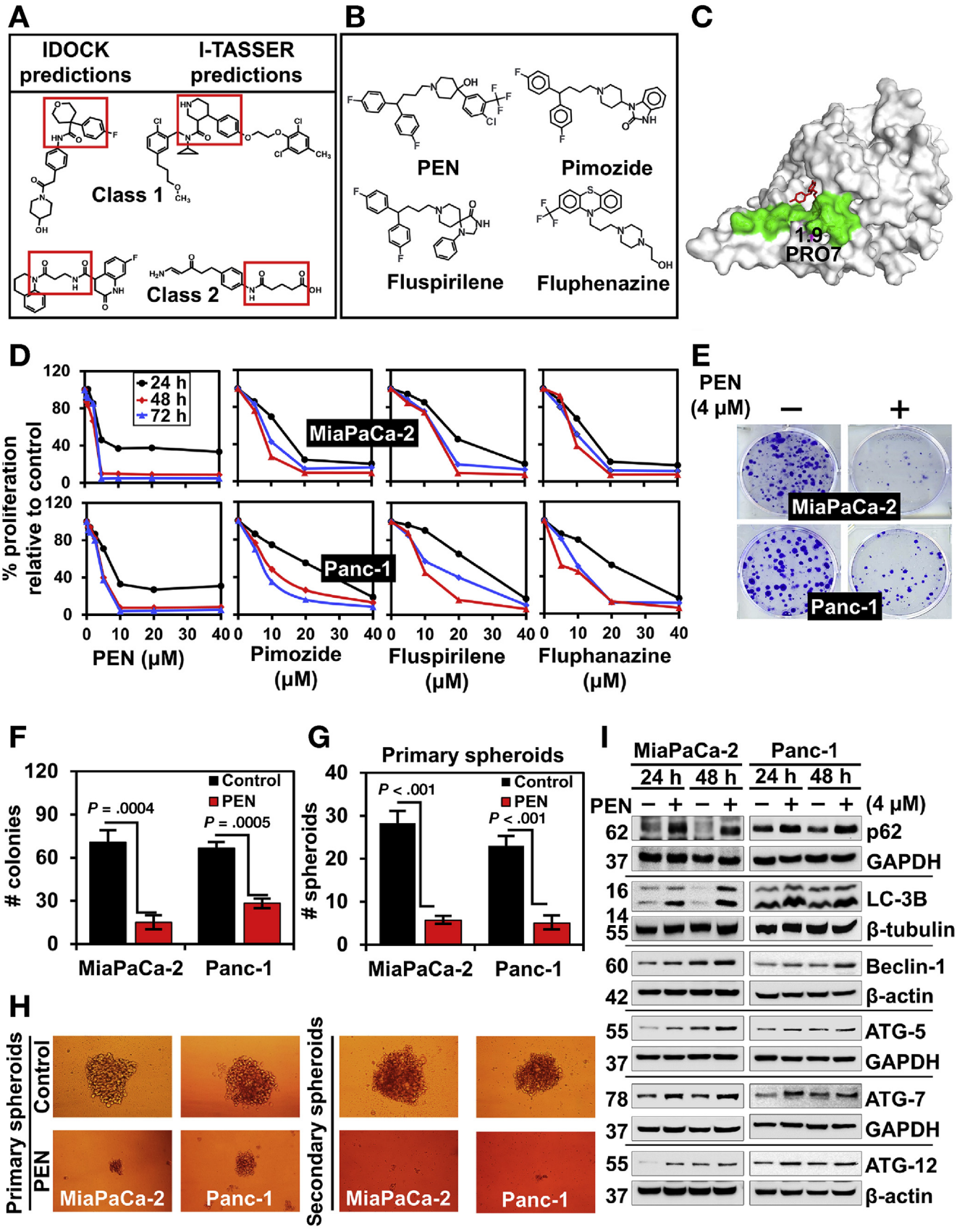

repeats (CRISPR)/Cas9 system. Although multiple clones were tested for each cell line, a complete knockout was not successful. We chose 1 clone each for MiaPaCa-2 and UNKC-6141 cells, named M64 and U518, respectively, to further knock down the expression using PRLR-specific short hairpin (shRNA). We observed maximum suppression of PRLR expression when we combined CRISPR/Cas9 and specific shRNA (Figure 3*A*). However, all the clones (CRISPR alone, shRNA alone, and the combination) showed lack of JAK2, STAT3, ERK, and AKT phosphorylation in response to PRL (Figure 3*B* and Supplementary Figure 3*A*). CRISPR and shRNA PRLR knockdown also reduced PDAC proliferation compared with controls (Supplementary Figure 3*B*). Moreover, there was a significant reduction in the colony (2 dimensional) and spheroid (3-dimentional) sizes compared with controls (Figure 3*C*–*E*). In addition, PRLR knockdown impaired cell migration (Figure 3*F* and Supplementary Figure 3*C*). Taken together, these data suggest that PRLR signaling is important for PDAC growth and migration. This is in line with previous studies showing that antagonizing PRLR results in reduced ovarian tumor growth in mice.[23] To determine the effect of PRLR knockdown in vivo, we used a syngeneic orthotopic model. We injected control UNKC-6141 cells, or their CRISPR clone U518 cells expressing scrambled or PRLR-specific shRNA, into the pancreas of C57BL/6 mice. UNKC-6141 control cells formed large tumors compared with the PRLR knockdown clones (Figure 3*G* and Supplementary Figure 3*D*). Similarly, the U518 clone expressing a combination of CRISPR and PRLR shRNA (U518-sh) formed smaller tumors (Figure 3*G* and Supplementary Figure 3*D*). More importantly, mice with PRLR knockdown tumors had higher survival rates than mice with tumors expressing wild-type PRLR (Figure 3*H*). In addition, PRLR knockdown tumors have fewer proliferating cell nuclear antigen (PCNA)–positive nuclei, suggesting reduced cell proliferation (Supplementary Figure 3*E* and *F*). Furthermore, Western blot analyses of extracts from the residual PDAC tumors lacking PRLR showed decreased STAT3, ERK, and AKT phosphorylation compared with control tumors (Supplementary Figure 3*G*). These data show that PRLR is essential for pancreatic tumor formation and growth.

Identification of Antipsychotic Agents as Prolactin Receptor–Interacting Compounds

Previous clinical studies with PRLR-specific peptide or antibody antagonists showed poor clinical efficacy, in part because they target the extracellular domain.[26] We chose a different approach, wherein we targeted the intracellular domain of PRLR responsible for downstream JAK2 activation. However, the intracellular domain of PRLR has not been crystallized.[27] Hence, we used homology-modeling algorithms (I-TASSER, SWISS modeler, RaptorX, and Phyre2) to predict the structure and evaluated by Ramachandran plot (Supplementary Figure 4*A* and *B*). Next, we performed structure-based virtual screening of compounds in I-TASSER and idock servers and identified 2 classes of compounds with potential binding capacity (Figure 4*A*). Subsequently, using a fragment-based drug discovery approach,[28,29] we identified 6 compounds with similarity to the 2 classes of predicted compounds (Figure 4*B* and Supplementary Figure 4*C*). We confirmed that the compounds can interact with the PRLR–JAK2 domain by molecular docking (Figure 4*C* and Supplementary Figure 4*D*). However, only 1 compound, penfluridol, showed interaction within the JAK2 binding domain; the others had allosteric interactions outside the JAK2 binding domain (Supplementary Figure 4*D*). Because penfluridol is an antipsychotic compound, we selected additional antipsychotic drugs belonging to chemical classes of butyrophenones (haloperidol and pipamperone), diphenylbutylpiperidines (fluspirilene and pimozide) and phenothiazines (promethazine and fluphenazine) (Figure 4*B* and Supplementary Figure 4*E*). Of these, only promethazine and fluspirilene showed interaction within the JAK2 binding domain; the others had allosteric interactions outside the JAK2 binding domain (Supplementary Figure 4*E*). Moreover, promethazine, penfluridol, and fluphenazine showed lower binding energies (Supplementary Figure 4*F*), indicating tight binding to the JAK2 binding site. Nevertheless, we tested all

Figure 4. In silico molecular modeling identifies penfluridol as a PRLR-interacting compound. (*A*) The JAK2 binding region within the cytoplasmic domain of PRLR was subjected to homology modeling using I-TASSER and was subsequently used for predicting potential interacting compounds with idock and I-TASSER. The predicted structure and their common features are shown in red boxes. (*B*) Fragment-based drug discovery was used to identify compounds targeting PRLR based on common structural features shown in the red boxes of panel *A*. The panel shows the most potent antipsychotic drugs identified, including penfluridol, pimozide, fluspirilene, and fluphenazine. (*C*) Molecular docking of penfluridol performed with the JAK2 binding site (*green*) using AutoDock Vina software (Scripps Research Institute, San Diego, CA). (*D*) Antipsychotic drugs inhibit PDAC cell proliferation. Cells were incubated with increasing concentrations (0–40 μmol/L) of compound for 72 hours, resulting in a dose- and time-dependent decrease in cell proliferation compared with untreated controls. (*E*) Penfluridol inhibits colony formation. Cells were incubated with 4 μmol/L penfluridol for 48 hours and allowed to grow into colonies for 10 days. Incubation with penfluridol inhibits clonogenicity. (*F*) Penfluridol inhibits number of colonies compared with control in MiaPaCa-2 ($P = .0004$) and Panc-1 ($P = .0005$) cells. (*G*) Penfluridol inhibits spheroid formation assay. Penfluridol suppressed the number of pancospheres in both primary and secondary spheroids cultures ($P < .001$). (*H*) Cells were grown in spheroid growth media in ultra-low-adherent plates and treated with penfluridol (4 μmol/L) for 5 days. Penfluridol significantly decreased pancosphere formation. (*I*) Penfluridol induces autophagy. Lysates from MiaPaCa-2 or Panc-1 cells incubated with 4 μmol/L penfluridol were analyzed by Western blotting for LC3B; p62; ATG-5, -7, and -12; and beclin-1. Penfluridol-treated cells shows increased levels of all of these proteins. GAPDH, glyceraldehyde-3-phosphate dehydrogenase; h, hour; M, mol/L; PEN, penfluridol.

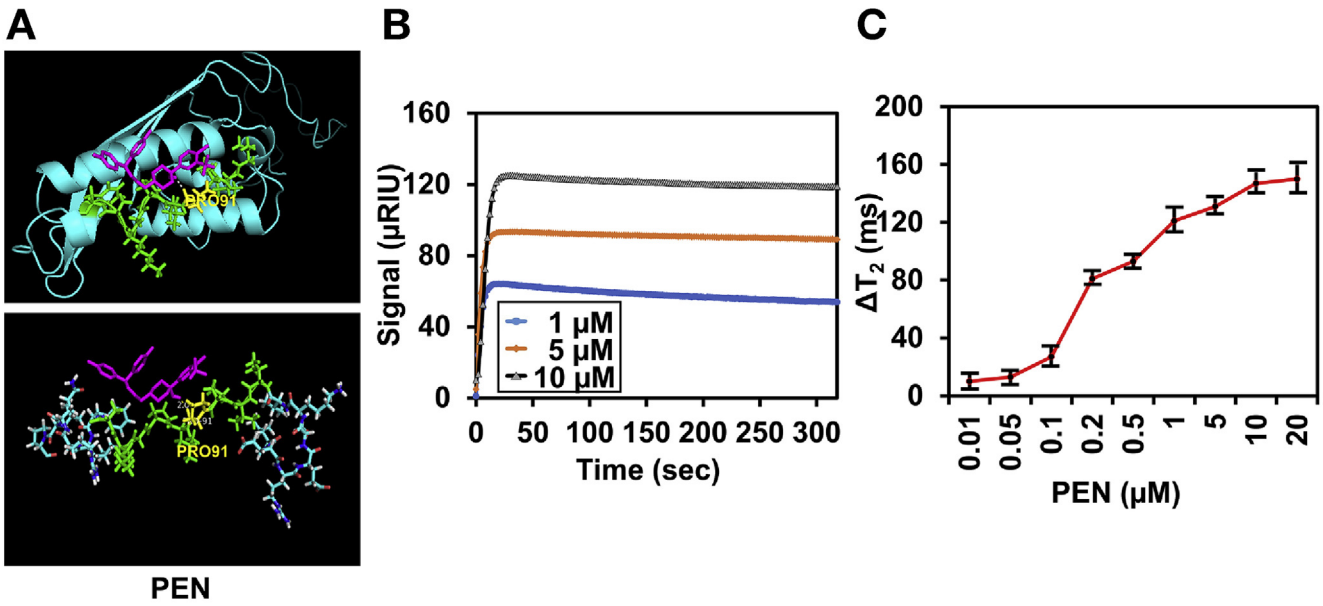

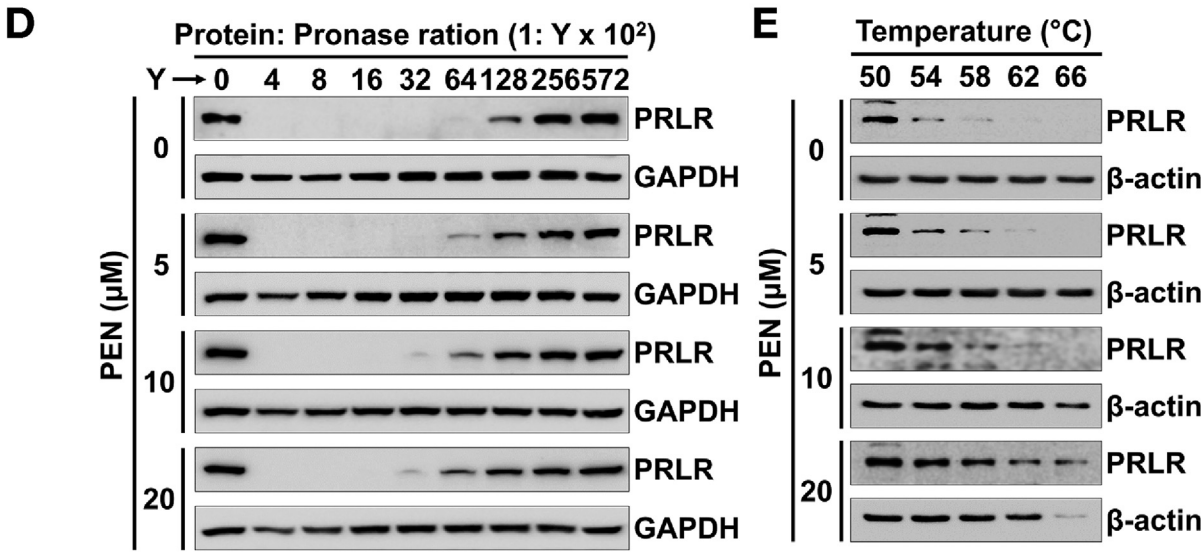

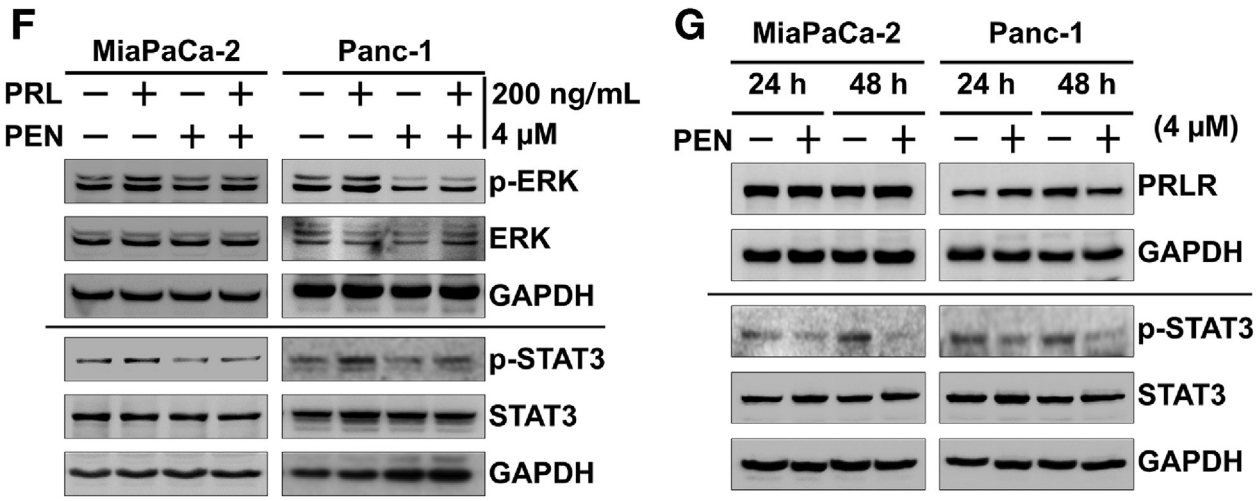

of the compounds for antiproliferative activity and observed that the antipsychotic compounds penfluridol, pimozide, fluspirilene, and promethazine were effective in suppressing proliferation (Figure 4*D* and Supplementary Figure 4*G*–*L*). Because penfluridol was the first antipsychotic that we identified, we chose this compound for proof-of-principle experiments. In addition to inhibiting PDAC cell proliferation, penfluridol suppressed colony and spheroid formation (Figure 4*E*–*H* and Supplementary Figure 4*M*). No other compound showed any effect on spheroid formation (Supplementary Figure 4*N* and *O*). Moreover, penfluridol suppressed cell proliferation even in the presence of exogenous PRL (Supplementary Figure 4*P*). Penfluridol induced autophagy at 48 hours, as evidenced by an increase in the expression of autophagy-related proteins (Figure 4*I*). Similarly, fluspirilene, promethazine, fluphenazine, and pimozide also increased levels of LC3II and p62 protein expression, indication up-regulation of autophagy (Supplementary Figure 4*Q*). However, penfluridol did not induce caspase activity, except at a higher concentrations (Supplementary Figure 4*R*). To confirm the specificity of the inhibitor, we treated PRLR-knockdown cells with penfluridol. PRLR-knockdown cells were resistant to penfluridol treatment, with a shift in the half maximal inhibitory concentration from 2–2.1 μmol/L to 3.2–3.8 μmol/L in MiaPaCa-2 and from 5.8–6 μmol/L to 7.4–7.6 μmol/L in UNKC-6141 cell lines (Supplementary Figure 4*S* and *T*). We also determined the effect of combining penfluridol with gemcitabine. There was synergistic activity observed in both MiaPaCa-2 and Panc-1 cell lines, with the best combination observed at a dose combination of 2.5 μmol/L penfluridol and 5.0 μmol/L gemcitabine (Supplementary Figure 4*U*–*W*).

Penfluridol Binds to Prolactin Receptor

Given that penfluridol affects cell viability, we further characterized its interaction with PRLR. In silico modeling showed penfluridol binding to the JAK2 domain of PRLR (Figure 5*A*). To validate the in silico observation, we first performed surface plasmon resonance (SPR) analyses with penfluridol and a PRLR peptide encoding the JAK2 binding site. Penfluridol binding to PRLR peptide on the surface of gold nanoparticles altered the local refractive index in a dose-dependent manner, resulting in a shift of the SPR spectrum (Figure 5*B*). We confirmed the direct binding of penfluridol with the PRLR peptide using magnetic relaxometry, a novel method where multivalent magnetic nanosensors are generated with the peptide.[30,31] Detection of the interaction between the peptide nanosensor and the compound is achieved by measuring changes in the solution's water relaxation times (ΔT2, measured in milliseconds) with a magnetic relaxometer. Initial studies with 0.5 μmol/L penfluridol showed a maximum interaction at 60 minutes (Supplementary Figure 5*A* and *B*). Using this time point, we determined the effect of increasing doses of penfluridol and observed a dose-dependent increase in the compound binding (Figure 5*C*).

We next validated the binding by treating PDAC cell lines with penfluridol and subjecting the cell to drug affinity responsive target stability assay and cellular thermal shift assay. Here, the target protein is subject to various lysis (drug affinity responsive target stability) or denaturation (cellular thermal shift assay) conditions with the assumption that a change in conformation after compound binding will result in an increase in its stability. We observed significant protection from pronase digestion (Figure 5*D*) and temperature (Figure 5*E*). On the other hand, penfluridol treatment did not change the stability of STAT3, confirming the specificity of penfluridol binding to PRLR (Supplementary Figure 5*C*).

We next determined the effect of penfluridol treatment on the JAK2–STAT3 signaling pathway. Pretreatment with penfluridol decreased PRL-induced ERK and STAT3 phosphorylation (Figure 5*F* and *G*). However, there was no effect on PRLR levels, suggesting that the compound does not induce degradation of the protein. Furthermore, we also found that antipsychotic drugs, including fluphenazine, fluspirilene, pimozide, and promethazine, inhibited PRL-induced STAT3 and ERK phosphorylation in the MiaPaCa-2 cell line (Supplementary Figure 5*D*).

Penfluridol Induced Suppression of Pancreatic Ductal Adenocarcinoma Growth Is Not Mediated Through Dopamine Receptor D2

DRD2 is present in the normal pancreas and is up-regulated in PDAC.[17] Penfluridol exerts its antipsychotic activity by blocking DRD2.[32,33] Molecular docking studies show that penfluridol binds the DRD2 protein, stabilizing the interaction by forming a hydrogen bond with ASP114

Figure 5. Penfluridol binds to PRLR. (*A*) Molecular docking shows that penfluridol binds to the JAK2 binding site of PRLR. Cartoon format of binding model (*upper panel*) and ball-and-stick format of model (*lower panel*) (protein: *blue*, penfluridol: *pink*, JAK2 binding site: *green*, interacting amino acid: *yellow*) are shown. (*B*) Dose-dependent (10 nmol/L–20 μmol/L) increase in penfluridol binding to PRLR calculated by SPR, RIU, Refractive index unit. (*C*) Dose-dependent (10 nmol/L–20 μmol/L) increase in penfluridol binding to PRLR calculated by the magnetic resonance technique. (*D*) drug affinity responsive target stability. MiaPACa-2 cells were treated with increasing concentrations of penfluridol (0–20 μmol/L) and then with pronase. The resulting lysates were subjected to Western blot analyses. Penfluridol protected PRLR against pronase-induced cell lysis, showing PEN–PRLR interaction. (*E*) Cellular thermal shift assay. MiaPACa-2 cells were treated with different concentrations of penfluridol and subjected to differential temperature treatments for 3 minutes. Western blot shows that penfluridol protected PRLR against thermal denaturation, suggesting compound interaction with receptor. (*F*) Penfluridol inhibits PRL-induced ERK and STAT3 phosphorylation. Western blot analyses of cells lysates after penfluridol treatment show reduced ERK and STAT3 phosphorylation in response to penfluridol. (*G*) Western blot analysis PDAC cell lysates after penfluridol treatment shows that the compound does not affect PRLR protein levels but that it inhibits STAT3 phosphorylation. GAPDH, glyceraldehyde-3-phosphate dehydrogenase; h, hour; M, mol/L; PEN, penfluridol.

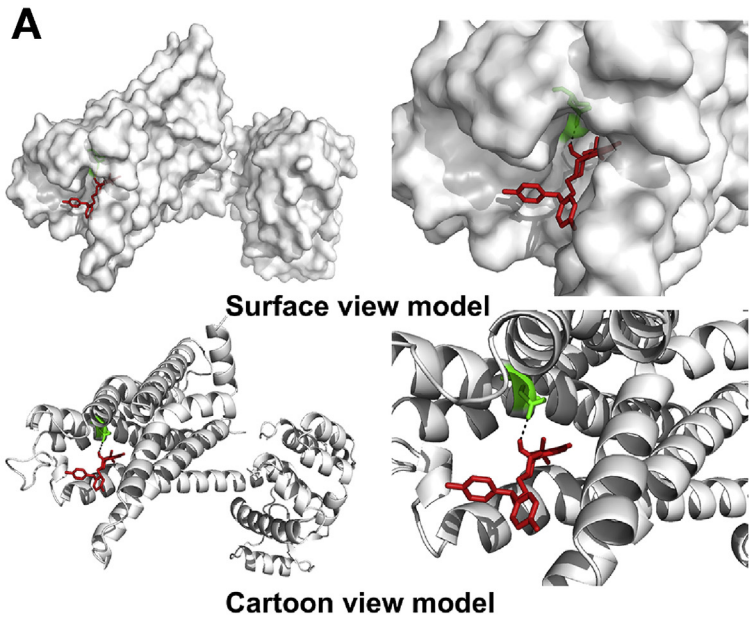

B

Compound	Penfluridol
B.E. (Kcal/mol)	-9.5
No H bonds	1
Amino acid	ASP114
Distance (Å)	2.6

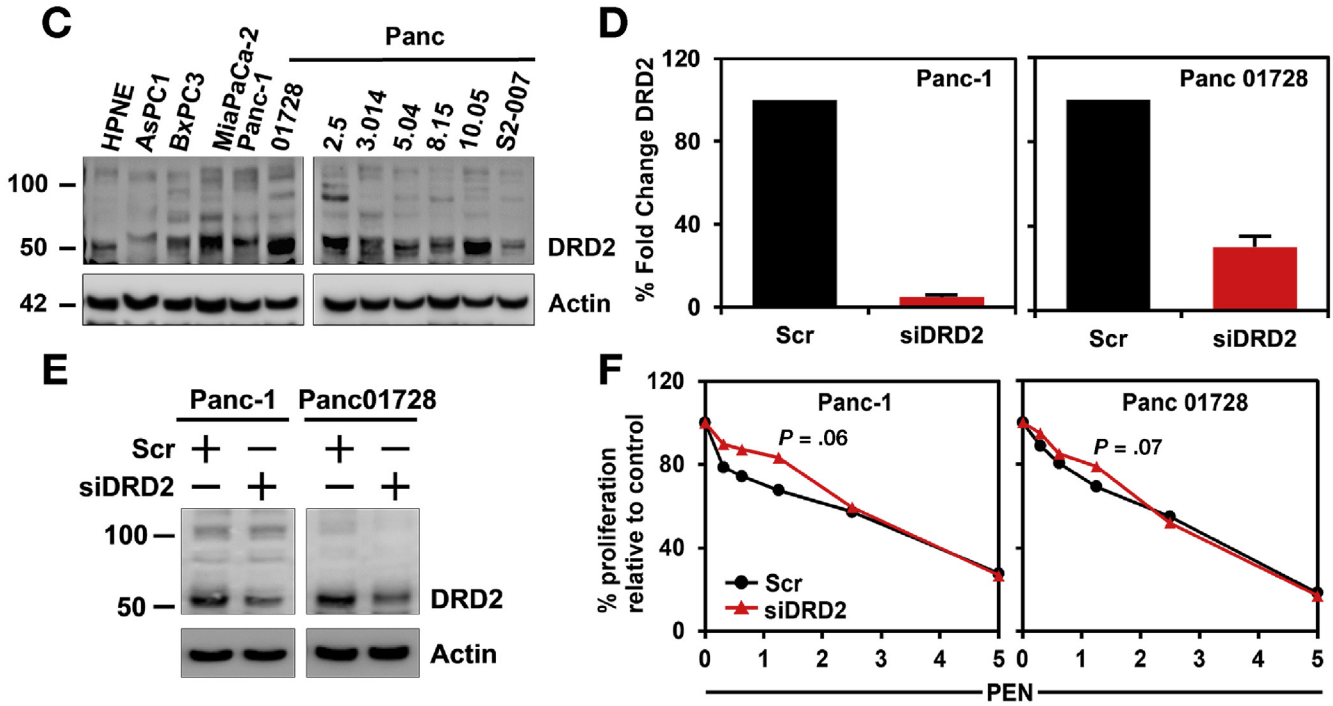

Figure 6. Penfluridol-induced suppression of PDAC growth is not mediated through DRD2 receptor. (*A*) Molecular docking of penfluridol was performed with DRD2 protein by using AutoDock Vina software. (*B*) Table showing docking scores of molecular docking of penfluridol with DRD2. B.E., Binding energy. (*C*) Western blot analysis shows that DRD2 is up-regulated in PDAC cell lines. (*D*) real-time polymerase chain reaction analysis showing knockdown of DRD2 expression induced by small interfering RNA (siRNA) in Panc-1 and Panc 01728 cell lines. (*E*) Western blot analysis showing siRNA-mediated knockdown of DRD2 expression. (*F*) Penfluridol does not have any differential effect in proliferation of PDAC cells when DRD2 is knocked down. PEN, penfluridol; Scr, scrambled.

(Figure 6*A* and *B*). Previously, another DRD2 antagonist, risperidone, was also shown to bind to ASP114, suggesting that binding to this site is the potential mechanism of action of penfluridol.[34] To understand the role of DRD2 in penfluridol inhibition of PDAC cell growth, we first determined the DRD2 expression levels. Western blot analysis of PDAC cell lines showed an increase in DRD2 protein expression compared with HPNE cells (Figure 6*C*). Although the major band indicating DRD2 is found at 52 kDa, there are multiple weak bands observed between 85 and 100 kDa, suggestive of DRD2 isoforms.[35] We next knocked down DRD2 using specific small interfering RNA in 2 PDAC lines, Panc-1 and Panc 01728, resulting in reduction in both DRD2 mRNA and protein ($P < .01$) (Figure 6*D* and *E*). However, penfluridol treatment did not show any significant difference in antiproliferative activity after DRD2 knockdown, although

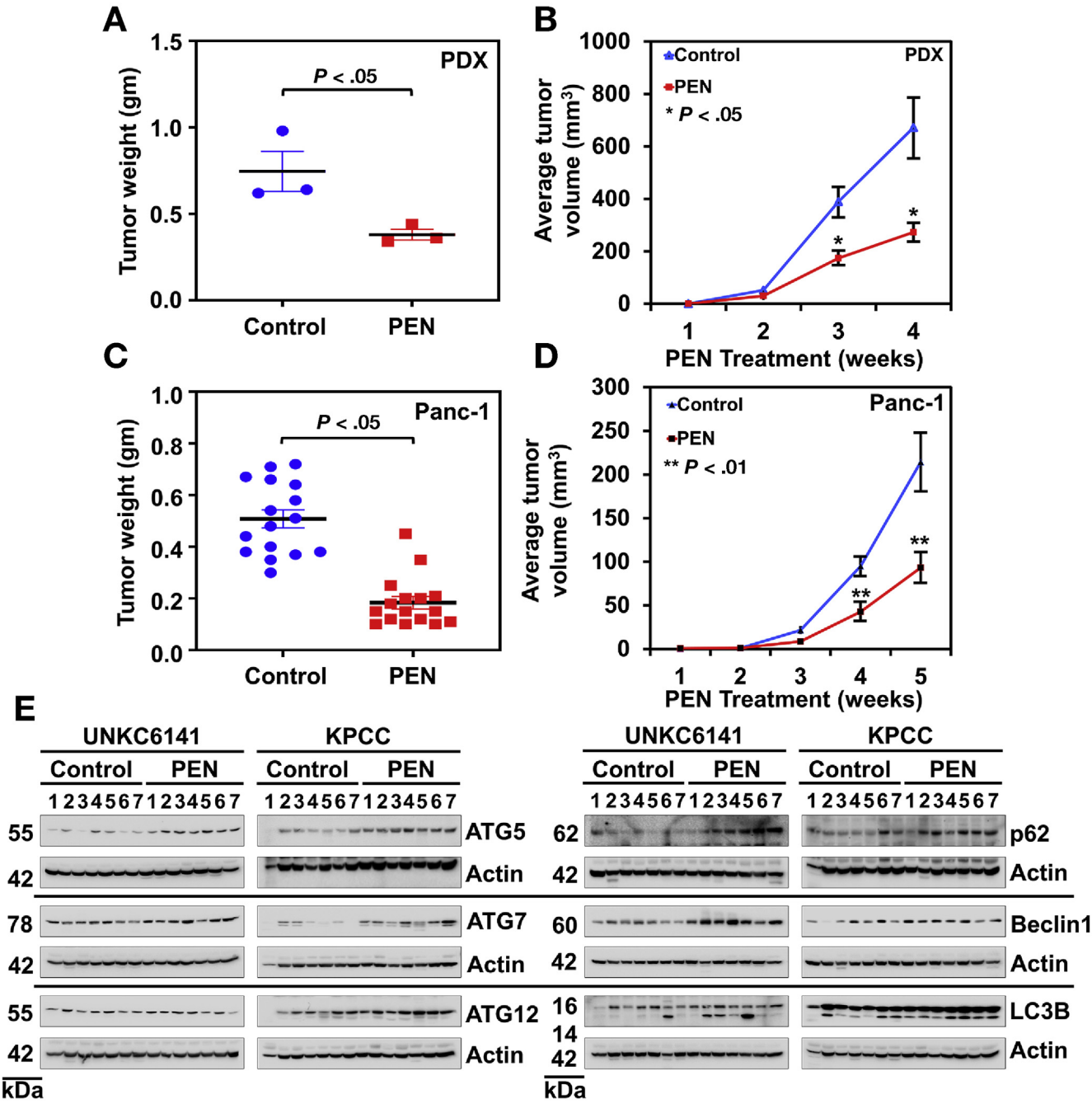

Figure 7. Penfluridol suppresses PDAC growth in vivo. (*A*) Penfluridol treatment reduced PDX tissue from patients with pancreatic cancer grown subcutaneously in the flanks of the NSG mice compared with controls ($P < .05$). (*B*) Penfluridol treatment resulted in significantly lower PDX tumor volumes compared with controls ($P < .05$). (*C*) Penfluridol treatment reduced Panc-1 tumor xenografts ($P < .01$) compared with controls. (*D*) Penfluridol treatment resulted in significantly lower Panc-1 xenograft tumor weight compared with controls ($P < .01$). (*E*) Western blot analyses of tissue lysates from penfluridol-treated animals show significantly higher levels of autophagy protein markers.

at 1 concentration (1.5 μmol/L), there was a small but insignificant effect (Figure 6*F*). This suggests that DRD2 is not a potential target for penfluridol in suppressing PDAC growth.

Penfluridol Suppresses PDAC Growth In Vivo

To determine the effect of penfluridol on tumor growth, we injected UNKC-6141 and KPCC cells into the pancreas of immunocompetent C57BL/6 mice and waited 1 week for tumors to develop. Subsequently, we injected penfluridol (5 mg/kg intraperitoneally daily), which reduced the weights of orthotopic tumors by more than 50% compared with control tumors (Supplementary Figure 6*A*–*C*). Next, we performed subcutaneous xenograft models with PDX and Panc-1 xenografts in immunodeficient NSG and athymic nude mice, respectively. Penfluridol treatment significantly

reduced tumor weight and volume in both xenograft tumors (Figure 7*A*–*D* and Supplementary Figure 6*D* and *E*). Immunohistochemistry also showed significantly lower proliferating cell nuclear antigen (PCNA)–positive cells in penfluridol-treated tumors (Supplementary Figure 6*F* and *G*). Western blot analyses suggested that penfluridol induced autophagy-related proteins p62, ATG-5, ATG-7, ATG-12, LC3B, and beclin-1 (Figure 7*E*). These data suggest that antipsychotic agents such as penfluridol significantly induce autophagy, resulting in suppression of PDAC tumor growth.

Discussion

To our knowledge, this is the first demonstration of the role of PRLR in PDAC, a deadly cancer with a very low 5-year survival rate. PRL can be produced by both the anterior pituitary gland and other tissues including mammary glands, adipocytes, pancreatic β cells, and immune cells to produce autocrine effects.[36] In normal tissue, PRL signaling is important for pancreatic β-cell proliferation.[37] Previous studies have focused on PRLR activity in hormone response cancers. Although PRLR in PDAC has not been demonstrated, elevated serum PRL levels have been reported,[10] suggesting a role for this signaling pathway in PDAC. Moreover, using Gene Analytics, we show that 22% of all published reports on PDAC pertain to molecules associated with PRLR signaling. Probing the TCGA database also showed higher PRLR expression in PDAC, which we validated using a complementary DNA panel and tissue microarray. These results indicate that PRLR has a role in PDAC pathogenesis.

PRL binds to its cognate receptor (PRLR) and activates downstream signaling pathways, including JAK–STAT and MAPK. Although previous reports suggested that PRLR induces JAK2-mediated STAT5 phosphorylation in breast[38] and ovarian[23] cancer cells, we did not observe STAT5 activation. Interestingly, it was shown that STAT5 and STAT3 mediate opposing effects, and activation of both STAT3 and STAT5 at the same time results in reduced proliferation of breast cancer cells.[39] In our study, we observed dose-dependent phosphorylation of STAT3. In addition, we observed that PRL did not affect PDAC cell proliferation. However, PRL did increase stemness and migration in PDAC, which we also previously observed in colon cancer cells.[5] Similar results have been reported for ovarian cancer, where PRL failed to induce proliferation.[23] Moreover, PRL has been shown to suppress cell death and enhance survival in various cancers.[3]

Patients with PDAC reported elevated psychological distress compared with those with other cancers.[40] Indeed, under conditions of stress, there is increased production of pituitary PRL and higher circulating PRL levels.[41] PRL plays key roles in the stress response by suppressing the hypothalamic–pituitary–adrenal axis and weakening the immune system.[42] Although the evidence for psychological stress causing cancer may be weak, those under stress may cultivate certain unwanted behaviors, including smoking, overeating, and decreased exercise, resulting in increased cancer risk. In addition, studies have shown that mice subjected to stress have significantly larger tumors, angiogenesis, and increased metastasis.[43] Moreover, antidepressants, antihypertensive agents, and drugs that increase bowel motility are known to induce hyperprolactinemia by acting through suppressing DRD2 activity.[44] A recent study also showed that stress accelerates PDAC[45] in a mouse model by inducing catecholamines, which were suppressed by the nonselective β-adrenergic receptor blocker propranolol. In fact, previous studies have shown that β-adrenergic receptor agonists can induce PRL secretion from pituitary cells and pre-adipocytes, which can be reversed by an antagonist such as propranolol.[46] Taken together, these data raise the question of whether inhibition of aggressive PDAC behavior may be due, in part, to the β-blocker reduction of PRL levels.

To get further insights into the role of PRLR in PDAC, we first used the CRISPR/Cas9 system to knock out the gene. However, after repeated testing, we were unable to obtain a complete knockout. We considered problems such as short guide RNA design, delivery methods, off-target effects, and homology-directed repair.[47] To overcome the shortcomings with guide RNA design, we generated multiple guide RNAs, but the results were the same. To eliminate the potential for off-target effects, we designed scrambled controls. Finally, we tried multiple ways to deliver the guide RNAs, including transfection reagents and lentiviral systems. Because none of these worked, we believe that it is not the system but, rather, the increased copy number at the gene loci or the potential presence of pseudogenes. However, subsequent knockdown with specific shRNA mitigated PRLR function in the cells, resulting in reduced proliferation, clonogenicity, migration, and pancosphere formation capacity.

Given the aggressive role of PRLR in PDAC growth, we conclude that it is an excellent therapeutic target. Previously, 2 PRLR antagonists, peptide G129R and monoclonal antibody LFA102, were reported. G129R is a novel antagonist peptide of PRL that inhibited PRL/PRLR signaling and reduced tumor growth in an orthotopic mouse model of ovarian cancer.[23] However, this has not progressed toward clinical trials, possibly due to stability issues on systemic delivery of the peptide. A second inhibitor, LFA102, is a monoclonal antibody, but clinical trials in breast and prostate cancer failed.[48] However, this might be for a couple of reasons. One is the potential unanticipated compensatory changes of downstream signaling pathways or up-regulation of other compensatory tumorigenic signaling pathways in response to PRLR inhibition. A second reason could be that the receptor is present intracellularly in cancer cells. Hence, targeting the extracellular domain may not be an effective strategy. Therefore, we believe that targeting the intracellular domain may be a better approach. We have observed that multiple antipsychotic agents can bind PRLR and affect cell viability. As proof of principle, we have taken penfluridol in our subsequent studies. We show that penfluridol targets the JAK2 binding site in PRLR, thereby suppressing JAK2–STAT3 and ERK/AKT signaling (Supplementary Figure 7). Penfluridol is a Food and Drug Administration–approved, long-lasting, and orally bioavailable drug used for the treatment of schizophrenia.[49] Recent reports have shown that penfluridol has anticancer properties against

breast cancer[50,51] and PDAC,[52] but the mechanism of action has not been fully described. We have now determined that this inhibition is through suppression of PRL signaling. In addition, we have also observed that fluspirilene and promethazine have similar activity. Because these are approved as antipsychotic medications by the US Food and Drug Administration, further research into these compounds is warranted to determine clinical efficacy. Previous studies have identified that DRD2, also a target for these antipsychotic agents, is up-regulated in PDAC and may play a role in growth of the tumor.[17] However, in our current studies, penfluridol did not appear to affect cells where DRD2 expression was suppressed. This is similar to another study that reported that thioridazine, also a DRD2 antagonist, inhibits the proliferation of breast cancer cells but is independent of DRD2 receptor expression.[53] This suggests that the antipsychotic agents function to inhibit PDAC growth exclusively through PRLR. Finally, growth hormone receptor can also activate JAK2-mediated signaling.[54] It would be interesting to determine whether these compounds also interfere with GHR (Growth hormone receptor)-JAK2 interaction, or whether the compound has a unique activity against PRLR. These are part of the future directions of the project.

Supplementary Material

Note: To access the supplementary material accompanying this article, visit the online version of *Gastroenterology* at www.gastrojournal.org, and at http://doi.org/10.1053/j.gastro.2019.11.279.

References

1. Goffin V, Binart N, Touraine P, et al. Prolactin: the new biology of an old hormone. Annu Rev Physiol 2002; 64:47–67.
2. Anderson TR, Pitts DS, Nicoll CS. Prolactin's mitogenic action on the pigeon crop-sac mucosal epithelium involves direct and indirect mechanisms. Gen Comp Endocrinol 1984;54:236–246.
3. Sethi BK, Chanukya GV, Nagesh VS. Prolactin and cancer: has the orphan finally found a home? Indian J Endocrinol Metab 2012;16:S195–S198.
4. Yeh YT, Lee KT, Tsai CJ, et al. Prolactin promotes hepatocellular carcinoma through Janus kinase 2. World J Surg 2012;36:1128–1135.
5. Neradugomma NK, Subramaniam D, Tawfik OW, et al. Prolactin signaling enhances colon cancer stemness by modulating Notch signaling in a Jak2-STAT3/ERK manner. Carcinogenesis 2014;35:795–806.
6. Dagvadorj A, Collins S, Jomain JB, et al. Autocrine prolactin promotes prostate cancer cell growth via Janus kinase-2-signal transducer and activator of transcription-5a/b signaling pathway. Endocrinology 2007;148:3089–3101.
7. Van Coppenolle F, Skryma R, Ouadid-Ahidouch H, et al. Prolactin stimulates cell proliferation through a long form of prolactin receptor and K+ channel activation. Biochem J 2004;377:569–578.
8. Asai-Sato M, Nagashima Y, Miyagi E, et al. Prolactin inhibits apoptosis of ovarian carcinoma cells induced by serum starvation or cisplatin treatment. Int J Cancer 2005;115:539–544.
9. Schroeder MD, Brockman JL, Walker AM, et al. Inhibition of prolactin (PRL)-induced proliferative signals in breast cancer cells by a molecular mimic of phosphorylated PRL, S179D-PRL. Endocrinology 2003;144: 5300–5307.
10. Levina VV, Nolen B, Su Y, et al. Biological significance of prolactin in gynecologic cancers. Cancer Res 2009; 69:5226–5233.
11. Siegel RL, Miller KD, Jemal A. Cancer statistics, 2019. CA Cancer J Clin 2019;69:7–34.
12. Burris HA 3rd, Moore MJ, Andersen J, et al. Improvements in survival and clinical benefit with gemcitabine as first-line therapy for patients with advanced pancreas cancer: a randomized trial. J Clin Oncol 1997;15:2403–2413.
13. Torres MP, Rachagani S, Souchek JJ, et al. Novel pancreatic cancer cell lines derived from genetically engineered mouse models of spontaneous pancreatic adenocarcinoma: applications in diagnosis and therapy. PLoS One 2013;8(11):e80580.
14. Ben-Ari Fuchs S, Lieder I, Stelzer G, et al. GeneAnalytics: an integrative gene set analysis tool for next generation sequencing, RNAseq and microarray data. OMICS 2016; 20:139–151.
15. Siegel RL, Miller KD, Jemal A. Cancer statistics, 2018. CA Cancer J Clin 2018;68:7–30.
16. Fitzgerald P, Dinan TG. Prolactin and dopamine: what is the connection? A review article. J Psychopharmacol 2008;22:12–19.
17. Jandaghi P, Najafabadi HS, Bauer AS, et al. Expression of DRD2 is increased in human pancreatic ductal adenocarcinoma and inhibitors slow tumor growth in mice. Gastroenterology 2016;151:1218–1231.
18. Trott JF, Hovey RC, Koduri S, et al. Alternative splicing to exon 11 of human prolactin receptor gene results in multiple isoforms including a secreted prolactin-binding protein. J Mol Endocrinol 2003;30:31–47.
19. Lopez-Pulido EI, Munoz-Valle JF, Del Toro-Arreola S, et al. High expression of prolactin receptor is associated with cell survival in cervical cancer cells. Cancer Cell Int 2013;13:103.
20. Cataldo L, Chen NY, Yuan Q, et al. Inhibition of oncogene STAT3 phosphorylation by a prolactin antagonist, hPRL-G129R, in T-47D human breast cancer cells. Int J Oncol 2000;17:1179–1185.
21. Gubbay O, Critchley HO, Bowen JM, et al. Prolactin induces ERK phosphorylation in epithelial and CD56+ natural killer cells of the human endometrium. J Clin Endocrinol Metab 2002;87:2329–2335.
22. da Silva PL, do Amaral VC, Gabrielli V, et al. Prolactin promotes breast cancer cell migration through actin cytoskeleton remodeling. Front Endocrinol (Lausanne) 2015;6:186.
23. Wen Y, Zand B, Ozpolat B, et al. Antagonism of tumoral prolactin receptor promotes autophagy-related cell death. Cell Rep 2014;7:488–500.

24. Ishiguro T, Ohata H, Sato A, et al. Tumor-derived spheroids: relevance to cancer stem cells and clinical applications. Cancer Sci 2017;108:283–289.
25. Friedl P, Hegerfeldt Y, Tusch M. Collective cell migration in morphogenesis and cancer. Int J Dev Biol 2004; 48:441–449.
26. Liu T, Joo SH, Voorhees JL, et al. Synthesis and screening of a cyclic peptide library: discovery of small-molecule ligands against human prolactin receptor. Bioorg Med Chem 2009;17:1026–1033.
27. Bugge K, Papaleo E, Haxholm GW, et al. A combined computational and structural model of the full-length human prolactin receptor. Nat Commun 2016;7:11578.
28. Erlanson DA. Introduction to fragment-based drug discovery. Top Curr Chem 2012;317:1–32.
29. Murray CW, Rees DC. The rise of fragment-based drug discovery. Nat Chem 2009;1:187–192.
30. Kaittanis C, Santra S, Perez JM. Role of nanoparticle valency in the nondestructive magnetic-relaxation-mediated detection and magnetic isolation of cells in complex media. J Am Chem Soc 2009;131:12780–12791.
31. Shelby T, Banerjee T, Zegar I, et al. Highly sensitive, engineered magnetic nanosensors to investigate the ambiguous activity of zika virus and binding receptors. Sci Rep 2017;7:7377.
32. Li P, Snyder GL, Vanover KE. Dopamine targeting drugs for the treatment of schizophrenia: past, present and future. Curr Top Med Chem 2016;16:3385–3403.
33. Tuan NM, Lee CH. Penfluridol as a candidate of drug repurposing for anticancer agent. Molecules 2019; 24(20):3659.
34. Wang S, Che T, Levit A, et al. Structure of the D2 dopamine receptor bound to the atypical antipsychotic drug risperidone. Nature 2018;555(7695):269–273.
35. Lee SP, O'Dowd BF, Rajaram RD, et al. D2 dopamine receptor homodimerization is mediated by multiple sites of interaction, including an intermolecular interaction involving transmembrane domain 4. Biochemistry 2003; 42:11023–11031.
36. Gorvin CM. The prolactin receptor: diverse and emerging roles in pathophysiology. J Clin Transl Endocrinol 2015; 2:85–91.
37. Arumugam R, Fleenor D, Freemark M. Knockdown of prolactin receptors in a pancreatic beta cell line: effects on DNA synthesis, apoptosis, and gene expression. Endocrine 2014;46:568–576.
38. Yang N, Liu C, Peck AR, et al. Prolactin-Stat5 signaling in breast cancer is potently disrupted by acidosis within the tumor microenvironment. Breast Cancer Res 2013; 15:R73.
39. Walker SR, Nelson EA, Yeh JE, et al. STAT5 outcompetes STAT3 to regulate the expression of the oncogenic transcriptional modulator BCL6. Mol Cell Biol 2013;33:2879–2890.
40. Jansen L, Hoffmeister M, Arndt V, et al. Stage-specific associations between beta blocker use and prognosis after colorectal cancer. Cancer 2014;120:1178–1186.
41. Lennartsson AK, Jonsdottir IH. Prolactin in response to acute psychosocial stress in healthy men and women. Psychoneuroendocrinology 2011;36:1530–1539.
42. Gala RR. The physiology and mechanisms of the stress-induced changes in prolactin secretion in the rat. Life Sci 1990;46:1407–1420.
43. Kim-Fuchs C, Le CP, Pimentel MA, et al. Chronic stress accelerates pancreatic cancer growth and invasion: a critical role for beta-adrenergic signaling in the pancreatic microenvironment. Brain Behav Immun 2014;40:40–47.
44. Molitch ME. Drugs and prolactin. Pituitary 2008;11:209–218.
45. Renz BW, Takahashi R, Tanaka T, et al. β2 adrenergic-neurotrophin feedforward loop promotes pancreatic cancer. Cancer Cell 2018;33:75–90.
46. Shin SH, Barton RE. Activation of the adrenergic beta-receptor stimulates prolactin release from primary cultured pituitary cells. Neuroendocrinology 1993; 57:670–677.
47. Peng R, Lin G, Li J. Potential pitfalls of CRISPR/Cas9-mediated genome editing. FEBS J 2016;283:1218–1231.
48. O'Sullivan CC, Bates SE. Targeting prolactin receptor (PRLR) signaling in PRLR-positive breast and prostate cancer. Oncologist 2016;21:523–526.
49. Soares BG, Lima MS. Penfluridol for schizophrenia. Cochrane Database Syst Rev 2006;2:CD002923.
50. Hedrick E, Li X, Safe S. Penfluridol represses integrin expression in breast cancer through induction of reactive oxygen species and downregulation of Sp transcription factors. Mol Cancer Ther 2017;16:205–216.
51. Ranjan A, Gupta P, Srivastava SK. Penfluridol: an antipsychotic agent suppresses metastatic tumor growth in triple-negative breast cancer by inhibiting integrin signaling axis. Cancer Res 2016;76:877–890.
52. Ranjan A, Srivastava SK. Penfluridol suppresses pancreatic tumor growth by autophagy-mediated apoptosis. Sci Rep 2016;6:26165.
53. Tegowski M, Fan C, Baldwin AS. Thioridazine inhibits self-renewal in breast cancer cells via DRD2-dependent STAT3 inhibition, but induces a G_1 arrest independent of DRD2. J Biol Chem 2018;293:15977–15990.
54. Zhang Y, Jiang J, Kopchick JJ, et al. Disulfide linkage of growth hormone (GH) receptors (GHR) reflects GH-induced GHR dimerization. Association of JAK2 with the GHR is enhanced by receptor dimerization. J Biol Chem 1999;274:33072–33084.

Received May 22, 2019. Accepted November 19, 2019.

Correspondence
Address correspondence to: Shrikant Anant, PhD, University of Kansas Medical Center, 3901 Rainbow Boulevard, Kansas City, Kansas 66160. e-mail: sanant@kumc.edu; fax: 913-588-4701.

Acknowledgments
Author contributions: Prasad Dandawate and Shrikant Anant designed and conceptualized the research. Prasad Dandawate performed in silico modeling experiments and identification of compounds. Prasad Dandawate, Gaurav Kaushik, David Standing, Chandrayee Ghosh, Afreen Asif Ali Sayed, Dharmalingam Subramaniam and Snoali Schoudhury performed in vitro and animal experiments. Prasad Dandawate, Tuhina Banerjee, and Santimukul Santra performed SPR and magnetic relaxometric experiments. Prasad

Dandawate, Ann Manzardo, and Merlin Butler performed and analyzed GeneAnalytics. Prasad Dandawate and Prabhu Ramamoorthy performed immunohistochemical (IHC) staining. Prasad Dandawate, Sufi Mary Thomas, and Shrikant Anant wrote the manuscript and analyzed the data. Ossama Tawfik evaluated and scored stained IHC slides. Domenico Coppola and Mokenge Malafa provided PDAC TMA and evaluated and scored stained IHC slides. Animesh Dhar, Subhash B. Padhye, Joaquina Baranda, Anup Kasi, Weijing Sun, Shahid Umar, Michael J. Soares, Scott J. Wier, Roy A. Jensen, Sufi Mary Thomas, and Shrikant Anant helped with experimental design and interpretation of data. Shrikant Anant also supervised all research. All authors read the manuscript and approved the study.

Conflicts of interest
The authors disclose no conflicts.

Funding
This work was supported by a pilot grant from the National Cancer Institute–designated University of Kansas Cancer Center (P30CA168524 to Shrikant Anant), National Institutes of Health grants (R01CA182872 and R01CA190291 to Shrikant Anant), Kansas IDeA Networks of Biomedical Research Excellence (K-INBRE, P20GM103418 to Prasad Dandawate), and University of Kansas Medical Center (KUMC) Biomedical Sciences Training Program (BRTP) (Prasad Dandawate), Frontiers Equipment award (KUMC, Prasad Dandawate). Shrikant Anant is an Eminent Scientist of the Kansas Biosciences Authority. We also thank the Thomas O'Sullivan Foundation and the Rod Rogers Foundation for providing financial support. The Flow Cytometry Core Laboratory and biospecimen repository are funded, in part, by National Institutes of Health grants NCRR P20 RR016443 and P30CA168524.

Supplementary Materials and Methods

Cells and Reagents

Human pancreatic cancer cells AsPC-1, BxPC-3, Panc-1, MiaPaCa-2 (all cell lines obtained from American Type Culture Collection) at passage 4 Panc 2.15, Panc 3.014, Panc 5.04, Panc 8.13, and Panc 10.05 were gifts from *Johns Hopkins* University. The S2-007 and UNKC-6141 cell lines were gifts from Dr Animesh Dhar and Dr Surinder Batra, respectively. The cell lines were grown in RPMI 1640 or DMEM with 4.5 g/L glucose, L-glutamine, and sodium pyruvate (Corning) containing 10% heat-inactivated FBS (Sigma-Aldrich) and 1% antibiotic-antimycotic solution (Corning) at 37°C in a humidified atmosphere of 5% CO_2. HPNE cells were kindly provided by Dr Anirban Maitra, MD Anderson Comprehensive Cancer Center. All the cell lines used in this study were within 20 passages after receipt or resuscitation (approximately 3 months of noncontinuous culturing). Penfluridol, LY255582, 4-acetylglutaranilic acid, 5-{4-[(tert-butylamino)-carbonyl]-anilino}-5-oxopentanoic acid, 4-(ethoxycarbonyl)-glutaranilic acid, and 4-butylglutaranilic acid (BG) were purchased from Sigma-Aldrich, and PRL was purchased from R&D Systems (Minneapolis, MN). For evaluating the effects of PRL, the cells were cultured in serum-free media for 24–48 hours before treatment with PRL (200 ng/mL). When indicated, cells were pretreated with penfluridol. Ferric chloride hexahydrate, ferrous chloride tetrahydrate, hydrochloric acid, and ammonium hydroxide were obtained from Thermo Fisher Scientific (Waltham, MA). Dimethylformamide (DMF), dimethyl sulfoxide (DMSO), polyacrylic acid (PAA), *N*-hydroxysuccinimide (NHS), and other chemicals were purchased from Sigma-Aldrich and used as received. The 1-ethyl-3-(3-[dimethylamino] propyl) carbodiimide hydrochloride (EDC) was obtained from Pierce Biotechnology (Rockford, IL). The 2-(*N*-morpholino)ethanesulfonic acid (MES) sodium salt from Acros Organics and the magnetic column were purchased from Miltenyi Biotec (Auburn, CA).

Proliferation and Apoptosis Assays

Pancreatic cancer cells were plated in 96-well plates, allowed them to grow for 24 hours, and were treated with increasing doses of respective compounds. Cell proliferation was measured by enzymatic hexosaminidase assay, as described previously.[1] For apoptosis, the Apo-one Homogeneous Caspase-3/7 Assay kit was used to calculate caspase 3/7 activity (Promega).

Clonogenicity Assay

Briefly, 350 viable pancreatic cancer cells per well were seeded in 6-well dishes and treated with penfluridol in 10% FBS containing RPMI1640/DMEM for 48 hours; then medium with or without compound was removed, and the cells were incubated for an additional 10 days in fresh complete medium to form colonies. The colonies were fixed with formalin and stained with crystal violet.

Western Blot Analysis

For Western blot analysis, pancreatic cancer cells were washed with phosphate-buffered saline (PBS) (3 times) and lysed in protein lysis buffer (Thermo Fisher Scientific) containing protease inhibitor (Roche, Basel, Switzerland). The resultant lysates were centrifuged at 6000 revolutions/minute for 10 minutes. Protein (30–75 μg) was loaded into gels. Cell lysates were subjected to polyacrylamide gel electrophoresis and transferred onto Immobilon polyvinylidene difluoride membranes (Millipore, Bedford, MA). These membranes were then blocked with 5% milk or 5% BSA and probed with different antibodies. The specific proteins were detected by the enhanced chemiluminescence system (GE Health Care, Piscataway, NJ). Protein expression was captured by the Bio-Rad (Hercules, CA) ChemiDoc-XRS+ instrument and analyzed by image lab software. PRL (sc-48383), PRLR (sc-20992), and GAPDH (sc-365062) were purchased from Santa Cruz Biotechnology (Dallas, TX); p-ERK (Thr202/Tyr204) (9101), ERK (4696), p-STAT3 (Tyr705) (9131), STAT3 (4904), p-JAK2 (Tyr1007/1008) (3776), JAK2 (3230), p-Akt (Ser473) (9271), AKT (9272), LC3B (2775), p62 (8025), ATG-5 (12994), ATG-7 (8558), ATG-12 (4180), beclin-1 (3738), and and Bcl2 (15071) were purchased from Cell Signaling Technology (Beverly, MA); β-actin (A1978) was purchased from Sigma-Aldrich; and DRD2 antibody (ab85367) was purchased from Abcam (Cambridge, UK).

Pancosphere Assay

Cells were cultured in DMEM supplemented with 20 ng/mL bFGF 10 mL per 500 mL of 50× B27 supplement, epidermal growth factor 20 ng/ml (all from Life Technologies, Waltham, MA) at low densities (3000 cells/mL) in 96-well low-adhesion plates. Cells were treated with or without compounds. After 5 to 7 days, the number and size of pancospheres were determined. For second passages, cells were grown in the absence of these compounds. To evaluate the effects of PRL on spheroid formation, we reduced the amount of growth factors used in the culture conditions to prevent any growth-promoting effects by these growth factors, which can complicate the analyses, and to gain a better idea of the role of PRL in promoting spheroid formation.[2] Specifically, we used one fourth the doses of growth factors (epidermal growth factor, fibroblast growth factor), heparin, and B12 supplements that were recommended by earlier studies.[2] This is the minimal concentration of growth factors necessary for cells to grow as spheroids. Below this limit, the cells would aggregate and die. Pancosphere formation was assessed after 5–7 days, and the number and size of pancospheres were determined.

Scratch Plate Assay

Migration of pancreatic cancer cells was measured using an *in vitro* wound-healing assay (or scratch plate assay) performed in a 6-well plate (Becton Dickinson, Franklin Lakes, NJ). Briefly, cancer cells were seeded at a density of 5–10 $\times$ 10^4 cells per well, grown to nearly confluent

monolayers in 10% serum-supplemented DMEM/RPMI medium, and then starved overnight in a serum-free medium. Perpendicular wounds were scratched through the cell monolayer with a sterile 10-μL pipette tip. The cells were then washed twice very gently with PBS, and the scratched areas were photographed at $\times$4 or $\times$10 magnification with computer-assisted microscopy. PBS was removed and replaced with 2 mL of media with or without 10% Fetal bovine Serum (FBS) and/or PRL. After 12 hours in a humidified incubator at 37°C with 5% CO_2, cells were fixed with formalin, each well was photographed at $\times$4 and $\times$10 magnification, and the pictures analyzed.

Transwell Assay

Cancer cell chemotaxis was performed in a Boyden chamber consisting of a cell culture insert (8-μm pore polyethylene terephthalate membrane, seated in each well of a 24-well companion plate). A total of 2×10^4 cells were seeded in the upper chamber of an insert in serum-free media and positioned in a 24-well plate containing serum-free media. Prolactin was added to the medium in the upper chamber, and migration was carried out in a humidified incubator at 37°C with 5% CO_2 for 12 hours. Nonmigratory cells on the upper side of the insert were removed with a cotton swab. Then, cells were fixed with formalin and stained with 4′,6-diamidino-2-phenylindole. For quantification, randomly selected fields on the lower side of the insert were photographed and quantified.

Pancreatic Cancer Orthotopic Model in Mice

Five-week-old male C57BL/6 mice, purchased from The Jackson Laboratory, were used for in vivo experiments. They were maintained with water and standard mouse chow ad libitum, and were used in protocols approved by the University's Animal Studies Committee. Animals were injected with 1×10^6 UNKC-6141,[3] empty vector, and UNKC-6141 KD cells in the pancreas and were allowed to form a tumor. The tumors were allowed to grow for 4 weeks. In another experiment, 1 week after implantation, penfluridol (5 mg/kg body weight) was administered intraperitoneally daily for 21 days. At the end of treatment, the animals were euthanized, and the tumors were removed, weighed, and used for histology (H&E), immunohistochemistry, and Western blot studies.

Pancreatic Cancer Patient-Derived Xenograft Model

For the PDX model, we purchased PDX-carrying NSG mice from The Jackson Laboratory (TM01212). The cryopreserved tumor tissue obtained from patients with pancreatic cancer was cut into small pieces. The 6-week-old NSG mice were anesthetized, and then the tissue was implanted subcutaneously into the interscapular fat pad by making a shallow incision in the dorsal region. Once tumors were established, we started to treat the mice with penfluridol 5 mg/kg intraperitoneally for 28 days. Tumor size was measured weekly. At the end of treatment, the animals were euthanized, and the tumors were removed and weighed.

Panc-1 Xenograft Tumors in Mice

Five-week-old male athymic nude mice were procured from Charles River Laboratory and maintained with water and standard mouse chow ad libitum. All study protocols were approved by the University's Animal Studies Committee. In brief, 1×10^6 Panc-1 cells were injected in the left and right flank of the mice and allowed to grow a xenograft for a week. One week after injection, a palpable tumor was observed. Subsequently, penfluridol (5 mg/kg) was administered intraperitoneally for 35 days. Tumor volumes were measured weekly. At the end of treatment, the animals were killed, and the tumors were removed, weighed, and use for histology (H&E), immunohistochemistry, and Western blot studies.

Immunohistochemistry

Paraffin-embedded tissues were cut to 4-μm sections and deparaffinized, followed by antigen retrieval. The tissue sections were blocked with UltraVision Hydrogen Peroxide block for 10 minutes (Thermo Fisher Scientific). The slides were incubated with primary antibodies overnight at 4°C. PRL (ab64377), PRLR (35-9200), DRD2 (SAB4301831) antibody were purchased from Abcam, Thermo Fisher Scientific and Sigma Aldrich. The next day, the primary antibody was washed, and tissues were incubated with HRP Polymer Quanto for 10 minutes and then developed with a DAB Quanto Chromogen-Substrate mixture (Thermo Fisher Scientific). Finally, the slides were counterstained with hematoxylin. The slides were examined in Nikon (Tokyo, Japan) Eclipse Ti microscope under a $\times$20 objective. The multiorgan tumor microarray was purchased from Biomax (Rockville, MD; catalog number BCN963): multiple-organ carcinoma microarrays, containing 16 types of organ cancer with matched or unmatched adjacent normal tissue (esophagus, stomach, colon, rectum, liver, lung, kidney, breast, uterine cervix, ovary, bladder, lymph node, skin, brain, prostate, pancreas). We obtained a human PDAC tissue microarray from Moffitt Cancer Center (96 tumors and 54 normal pancreatic tissues) and the University of Kansas Medical Center (87 tumor and 3 normal pancreatic tissues).

Real-Time Reverse-Transcription Polymerase Chain Reaction Analysis

Pancreatic cancer complementary DNA panel with matched adjacent tissue controls was obtained from OriGene (Rockville, MD). Total RNA from cell lines was isolated using Trizol reagent (Invitrogen, Carlsbad, CA) following the manufacturer's instructions. We used 2 μg RNA to synthesize complementary DNA using Superscript II reverse transcriptase and random hexanucleotide primers (Invitrogen). Individual gene expression was quantified with SYBR green reagent (Molecular Probes, Eugene, OR) and specific primers with β-actin as an internal standard. Primers for the polymerase chain reaction (PCR) include 5′-

TGAACAAGTGCACCGAGTTG-3′ and 5′-AGTGAGTAAGGCAGAAAGCCC-3′ for PRLR and 5′-GACAACGGCTCCGGCAT-3′ and 5′-CTCGTCGCCCACATAGGAAT-3′ for β-actin, 5′-CAATACGCGCTACAGCTCCAAG-3′ and 5′-GGCAATGATGCACTCGTTCTGG-3′ for DRD2.

Homology Modeling and Molecular Docking

The x-ray crystal structure of the human PRL receptor intracellular domain structure is not available. Therefore, we used the homology-modeling approach to design a 3-dimensional (3D)structure by using the online server of I-TASSER (https://zhanglab.ccmb.med.umich.edu/I-TASSER/), SWISS modeler (https://swissmodel.expasy.org/interactive), and Phyre2 (http://www.sbg.bio.ic.ac.uk/phyre2/html/page.cgi?id=index).[4] We used the FASTA sequence of PRLR of the intracellular domain from UniProt (P16471) for homology modeling. The resulting 3D protein structure was evaluated with the PDBSUM-Generate online server and confirmed by Ramachandran plots (http://www.ebi.ac.uk/thornton-srv/databases/pdbsum/Generate.html). Interaction of compounds with PRLR was studied using the best-predicted 3D structure. To identify compounds interacting with PRLR in silico, we used the idock and I-TASSER online program, which yielded 2 compounds. Based on these compounds, we selected similar compounds available from Sigma-Aldrich and used them for further studies. All of the docking calculations were carried out with AutoDock Vina software[5] to analyze the compound interactions with the 3D structure PRLR. Later, the most stable conformation for compounds was selected based on the scoring function and the lowest binding energy and was visualized with PyMOL (https://pymol.org/2/).[6] AutoDock Vina is a free molecular docking program for faster drug discovery and virtual screening of drug molecules. It also offers high performance and increased accuracy compared with its previous versions. AutoDock Vina software is developed in Molecular Graphics Lab at The Scripps Research Institute (http://vina.scripps.edu/). It analyzes a rapid energy assessment through precalculated grids of affinity potentials and follows a variety of algorithms to determine suitable binding positions. The 3D grid box is generated containing all active site residues and a grid center coordinate consisting of grid spacing of 1.0 Å and 60 × 60 × 60 point size. All docking calculations were performed by using default parameters of the AutoDock tools. Total Kollman and Gasteiger charges were added to the protein and the ligand before docking. The Lamarckian genetic algorithm was used to find the best conformations. Approximately 10 conformations for each compound were selected. The interaction of penfluridol with the binding site of DRD2 was carried out with AutoDock Vina by using same protocol. The DRD2 protein structure was downloaded from the Protein Data Bank (identifier: 6CM4.pdb),[7] and the grid was generated around the risperidone binding site for docking.

Cellular Thermal Shift Assay

The ability of penfluridol to interact with and stabilize PRLR in cells was studied with the cellular thermal shift assay.[8] Briefly, MiaPaCa-2 cells were cultured and grown to 70%–80% confluence. The cell suspension was treated with media containing DMSO or penfluridol (5, 10, and 20 μmol/L) for 4 hours. After treatment, the cell suspension was aliquoted into PCR tubes and heated for 3 minutes at different temperature gradients. Subsequently, cells were lysed by using 2 repeated freeze–thaw cycles using liquid nitrogen, followed by centrifugation for 20 minutes. The resultant proteins were diluted with 4× Laemmli buffer, boiled at 70°C for 10 minutes and loaded onto 10% sodium dodecyl sulfate–polyacrylamide gel electrophoresis (SDS-PAGE) gel, transferred to polyvinylidene difluoride membrane, and incubated with PRLR antibody at a concentration of 1:1000. Protein levels on Western blot were pictured by the Bio-Rad ChemiDoc-XRS+ instrument and analyzed by Image Lab software (Bio-Rad).

Drug Affinity Responsive Target Stability

The ability of Penfluridol to interact with and stabilize PRLR in cells was studied by using drug affinity responsive target stability.[9] Cells were lysed by using M-PER (Mammalian Protein Extraction Reagent, Thermo Fisher Scientific) lysis buffer supplemented with protease inhibitor cocktail tablet, collected by scraping off with a cell scraper, and lysed on ice for 10 minutes, followed by centrifugation to pellet cell debris; supernatant was transferred to fresh tubes, followed by protein estimation using the bicinchoninic acid assay (BCA assay) method. Cell lysates were divided into equal-concentration aliquots and incubated with DMSO or penfluridol (5, 10, and 20 μmol/L) for 30 minutes with shaking. After incubation, respective lysates were divided into equal parts and treated with pronase (10 mg/mL) from 1:400; 1:800; 1:1600; 1:3200; 1:6400; 1:12,800; 1:26,000; and 1:57,000 protein:pronase ratio for 10–15 minutes. The protease digestion was stopped by using 20× protease inhibitor cocktail and further incubated for 10 minutes on ice. The resultant protein samples were diluted with 4× Laemmli buffer, boiled at 70°C for 10 minutes, loaded onto 10% SDS-PAGE gel, transferred to polyvinylidene difluoride membrane, and incubated with PRLR antibody at a concentration of 1:1000. Protein levels on Western blot were pictured by the Bio-Rad ChemiDoc-XRS+ instrument and analyzed by Image Lab software.

Small Interfering RNA Transfection

DRD2 knockdown in cancer cells was performed with a pool of 3 target-specific 19.25-nucleotide small interfering RNA (siRNA) (sc-35161, Santa Cruz Biotechnology). Transfection was performed using Lipofectamine-2000 (Invitrogen) and OptiMEM (Life Technologies) according to manufacturer recommendations. Briefly, cells were plated at 2×10^5 cells per well into 6-well plates or 5000 cells per well in 96-well plates and transfected by using either a combination of si scramble or siRNA. The concentration of siRNA used was 80 nmol/L. Lipofectamine-2000 (Invitrogen) was used as the transfection reagent. Six hours after transfection, cells were washed with PBS and treated with 10% serum containing DMEM. The knockdown was

confirmed with real-time PCR and Western blot at 24 and 48 hours after transfection, respectively. Twenty-four hours after siRNA transfection, cells were treated with penfluridol, and proliferation was measured with hexosaminidase assay. All data plotted were statistically analyzed.

Short Hairpin RNA Transduction

PRLR knockdown in cancer cells was done by using the lentiviral short hairpin RNA (shRNA) particles. shRNA plasmids for PRLR and scrambled were procured from Sigma-Aldrich. Lentiviral particles were generated using the pLVX Advanced plasmid system (ClonTech Laboratories, Mountain View, CA) in Lenti-X cells, transfected with the pGIPZ set of packaging plasmids generously donated by Roy Jensen. Pancreatic cancer cells were transduced with PRLR shRNA lentivirus, followed by selection with 10 mg/mL of puromycin (Life Technologies). Cells were consistently maintained in 0.4 μg/mL puromycin after selection unless otherwise noted.

Clustered Regularly Interspaced Short Palindromic Repeats–Cas9 Transfection

Knockout of the PRLR protein in pancreatic cancer cells was done by using the CRISPR/Cas9 gene editing tool. For this, the PRLR gene sequence was edited by targeting multiple sites in the PRLR gene for both human and mouse separately. Guide RNA sequences, specific to mouse and human PRLR genes, were procured from OriGene. For stable cell line development, donor plasmids with green fluorescent protein and puromycin resistance cassette inserts were used. Donor plasmid was inserted into the target genome sequence by using the homology directed repair (HDR) repair mechanism using guide RNA targeted sequences as a template for the insertion of donor plasmid. Guide RNA and donor plasmids were transiently transfected in pancreatic cancer cells lines (MiaPaCa-2 and UNKC-6141) using Lipofectamine 2000. Cells were grown in serum- and antibiotic-free media 18 hours before transfection. After 4 hours of transfection, the media was changed with complete media containing serum and antibiotics. Cells were further grown for 5 or 6 passages and were treated with puromycin for PRLR -knockout clone selection. PRLR-knockout clones were selected and used for further studies.

Magnetic Susceptibility Studies

The overall size and zeta potential of nanoparticles were measured by using dynamic light scattering studies with a Zetasizer Nano ZS90 from Malvern Instruments (Worcestershire, UK). Magnetic resonance data were collected using a benchtop magnetic relaxometer from Bruker (Billerica, MA), mq20, B = 0.47T (B = magnetic flux density, T = Tesla). The spin–spin magnetic relaxation times, designated as T2, were measured by using the magnetic relaxometry and expressed in milliseconds. For each magnetic relaxation experiment, a control sample was prepared and run parallelly to obtain the corresponding magnetic relaxation time; this was treated as a baseline. This value was deducted from the corresponding binding experiment data to obtain any effective binding, ΔT2.

Synthesis of Polyacrylic Acid–Coated Magnetic Nanosensor

Magnetic nanoparticles were synthesized by using the water-based precipitation method. Three solutions were prepared: (1) iron salt solution (0.9 g of $FeCl_3$ and 0.2 g of $FeCl_2$ in 2mol/L HCl solution), (2) alkaline solution (30% NH_4OH solution in N_2-purged deionized water), and (3) PAA solution in water. The iron salt solution was added to the alkaline solution, followed by the addition of the stabilizing agent. The reaction was continued for 60 minutes. Thereafter, the resulting magnetic nanosensor (MnS) was centrifuged to get rid of macro-sized particles and then purified with a magnetic column. The concentration of iron in the magnetic nanoparticles was determined with our previously reported procedure and was found to be 7.5 μmol/L. The overall size of the MnS was 71 $\pm$ 2 nm, with a polydispersity index of 0.28 and the negative zeta potential (ζ = –28 mV) confirmed for the presence of carboxylic acid groups (from PAA coatings) on the surface.

Synthesis of Prolactin Receptor Peptide–Conjugated Magnetic Nanosensor: Carbodiimide Chemistry

To synthesize PRLR peptide–conjugated MnS, 5 mL of MnS suspension was mixed with EDC (10 mmol/L) and mixed for 10 seconds, followed by NHS (10 mmol/L) in MES buffer (pH 6.0) added and incubated for 3 minutes at room temperature on a table mixer. Finally, PRLR peptide (10 mmol/L) in 500 μL of PBS (pH = 7.4) was added to the reaction mixture dropwise and kept for incubation at room temperature on the table mixer for a minimum of 3 hours. The resulting PRLR peptide–MnS suspension was purified by passing it through the magnetic column, washed with PBS, and suspended in PBS solution (pH = 7.4).

Surface Plasmon Resonance Spectroscopy

SPR experiments were performed with a Reichert (Buffalo, NY) SPR system SR7500DC at 25°C. The PRLR was captured on a CM5 sensor chip. To activate the sensor chip, a mixture of 40 mg/mL of EDC and 10 mg/mL NHS solution was injected. Next, a 10-minute injection of 1 mol/L ethanolamine pH 8.5 was used to block the unreacted sites on the sensor chip. Penfluridol at concentrations of 1, 5, and 10 μmol/L was perfused over the surface of PRLR at a flow rate of 50 μL/minute. After each injection, the surface of the chip was regenerated by injection of 10 mmol/L glycine at pH 1.5. Scrubber 2 software was used for data analysis. The equilibrium dissociation constant (K_D) determined from SPR analysis was 1.6 μmol/L.

The Cancer Genome Atlas (TCGA) Data

The TCGA data is extracted by using Xena browser, Firebrowse and the human tissue atlas.

Statistical Analysis

All values are expressed as the mean $\pm$ standard error of the mean. Data were analyzed with an unpaired 2-tailed t test. A P value of less than .05 was considered statistically significant.

References

1. Subramaniam D, Nicholes ND, Dhar A, et al. 3,5-bis(2,4-difluorobenzylidene)-4-piperidone, a novel compound that affects pancreatic cancer growth and angiogenesis. Mol Cancer Ther 2011;10:2146–2156.
2. Neradugomma NK, Subramaniam D, Tawfik OW, et al. Prolactin signaling enhances colon cancer stemness by modulating Notch signaling in a Jak2-STAT3/ERK manner. Carcinogenesis 2014;35:795–806.
3. Torres MP, Rachagani S, Souchek JJ, et al. Novel pancreatic cancer cell lines derived from genetically engineered mouse models of spontaneous pancreatic adenocarcinoma: applications in diagnosis and therapy. PLoS One 2013;8(11):e80580.
4. Kelley LA, Mezulis S, Yates CM, et al. The Phyre2 web portal for protein modeling, prediction and analysis. Nat Protoc 2015;10:845–858.
5. Trott O, Olson AJ. AutoDock Vina: improving the speed and accuracy of docking with a new scoring function, efficient optimization, and multithreading. J Comput Chem 2010;31:455–461.
6. Alexander N, Woetzel N, Meiler J. bcl::Cluster: a method for clustering biological molecules coupled with visualization in the Pymol Molecular Graphics System. IEEE Int Conf Comput Adv Bio Med Sci 2011;2011:13–18.
7. Wang S, Che T, Levit A, et al. Structure of the D2 dopamine receptor bound to the atypical antipsychotic drug risperidone. Nature 2018;555(7695):269–273.
8. Jafari R, Almqvist H, Axelsson H, et al. The cellular thermal shift assay for evaluating drug target interactions in cells. Nat Protoc 2014;9:2100–2122.
9. Pai MY, Lomenick B, Hwang H, et al. Drug affinity responsive target stability (DARTS) for small-molecule target identification. Methods Mol Biol 2015;1263:287–298.

A

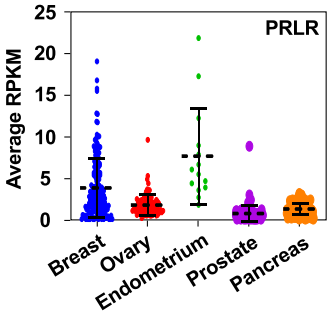

B

ACACA	IRS2	PPIB	CSH1	MAPK14	SHC4	GSK3B
AGAP2	ITGB1	PRKCD	CSH2	MAPK3	SIRPA	HRAS
AKT1	JAK1	PRL	CSN2	MAPK8	SLC2A2	IKBKB
AKT2	JAK2	PRLR	CTSD	MAPK9	SOCS1	PIK3CG
AKT3	JUN	PTK2	CYP17A1	MTOR	SOCS2	PIK3R1
BAX	KHDRBS1	PTPN1	EIF4EBP1	MYC	SOCS3	PIK3R2
BCL2	KPNA4	PTPN11	ELF5	NCOA1	SOCS4	VAV1
BCL2L1	KRAS	PXN	ELK1	NEK3	SOCS5	VAV2
CASP3	LEP	RAC1	EP300	NFKB1	SOCS6	YWHAG
CBL	LEPR	RAF1	ERBB2	NFKBIA	SOCS7	INS
CCND1	LHB	REL	ESR1	NFKBIB	SOS1	IRF1
CCND2	LHCGR	RELA	ESR2	NMI	SOS2	PLCG1
CDC42	LOC138159	RHOA	FLNA	NOS2	SP1	PLCG2
CEBPB	MAP2K1	RPS6	FOS	NR3C1	SRC	PPIA
CFL2	MAP2K2	RPS6KA2	FOXO1	NRAS	STAT1	IRS1
CGA	MAPK1	RPS6KB1	FOXO3	OAS1	STAT3	GRB2
CHUK	MAPK10	SH2B1	FYN	PAK1	STAT5A	PIK3CD
CISH	MAPK11	SHC1	GAB2	PDE3B	STAT5B	TNFSF11
CREB1	MAPK12	SHC2	GALT	PIAS3	TEC	IL1RN
CREBBP	MAPK13	SHC3	GCK	PIK3CA	TH	PIK3R5
GH1	PIK3CB	TNFRSF11A	IKBKG	PIK3R3	YWHAZ	ZAP70

C

Tissue and Cells	Score	Total genes	Matched genes	Percentage
Cerebral Cortex	3.9	5055	65	1.29
Pancreatic-like islets	**3.4**	**6**	**3**	**50**
Duodenum	3.0	3186	53	1.66
Villous Cytotrophoblast Cells	2.9	36	3	8.33
Medulla Oblongata	2.8	2179	35	1.60
Hematopoietic Bone Marrow	2.6	2063	42	2.03
Islet-like clusters	**2.6**	**4**	**2**	**50**
Ovary	2.6	1726	27	1.56
Beta-like cells	**2.5**	**10**	**3**	**30**

D

Disease	Score	Total genes	Matched genes	Percentage
Breast Cancer	36.33	742	47	6.3
Prostate Cancer	36.02	682	49	7.2
Colorectal Cancer	35.09	811	44	5.4
Lung Cancer	29.88	632	36	5.7
Endometrial Cancer	22.40	79	23	29.1
Pancreatic Cancer	**21.35**	**154**	**24**	**15.6**
Diabetes Mellitus, Noninsulin-Dependent	18.52	211	20	9.5
Leukemia, Acute Myeloid	17.61	188	19	10.1
Noonan Syndrome 1	16.31	16	9	56.3
Insulin-Like Growth Factor I	16.19	34	15	44.1
Organ System Cancer	14.14	83	15	18.1
Leukemia	13.50	28	9	32.1

Supplementary Figure 1. (*A*) Differential RNA expression of PRLR in various normal tissues. The samples were adapted from the Genotype-Tissue Expression (GTEx) data set. RNA-sequencing data are reported as median (in reads per kilobase per million mapped reads [RPKM]), generated by the GTEx project. (*B*) The PRLR pathway gene set used for analyses with the GeneAnalytics program (http://geneanalytics.genecards.org). (*C*) GeneAnalytics analysis: the top-ranked tissues and cells related to the PRLR pathway gene set. (*D*) GeneAnalytics analysis: the top-ranked diseases related to the PRLR pathway gene set. (*E*) Immunohistochemistry was used to evaluate PRLR expression in multiple cancer tissues (kidney, bladder, uterine cervix, lung, lymph node, skin, and brain). PRLR is differentially up-regulated in several cancers (N, normal; T, tumor). (*F*) Immunohistochemistry was used to evaluate PRLR expression in a PDAC tumor microarray obtained from Moffitt Cancer Center. Only β cells express high PRLR levels in normal pancreas. However, in tumors, PDAC cells show high levels of PRLR expression. (*G*) Immunohistochemistry was used to evaluate PRLR expression in pancreatic tumor (PCa) microarray from the University of Kansas Cancer Center. Pancreatic tumors show high levels of PRLR expression, whereas expression in normal pancreas is low. Again, pancreatic β cells express high PRLR levels in normal pancreas. (*H*) Immunohistochemistry: composite score shows significantly high expression of PRLR in tumor compared with normal pancreas ($P = .024$). (*I*) Immunohistochemistry: composite score shows significantly higher levels of PRLR expression in various differentiation status of PDAC compared with normal pancreas ($P < .05$). (*J*) Composite score of immunohistochemistry shows significantly higher expression of PRLR in the various stages of PDAC compared with normal pancreas ($p < .05$). (*K*) Immunohistochemistry: patient characteristics including sex, age, lymphovascular invasion (LVI), perineural invasion (PNI), and tumor size are independent of PRLR expression. The composite score is the sum of the level of PRLR staining and the number of PRLR-positive cells. (*L*) Differential gene expression of PRLR between normal and tumor patient samples obtained through the Firebrowse server. PRLR gene expression is high in tumor samples compared with normal samples of breast and pancreatic cancer (RSEM, RNA-Seq by Expectation Maximization). (*M*) Differential expression of prolactin (PRL) mRNA in the various normal tissues adapted from the GTEx data set. RNA-sequencing data are reported as median RPKM, generated by the GTEx project. (*N*) PRL RNA-sequencing data in cancer types are reported as median number of fragments per kilobase of exon per million reads (FPKM), generated from data obtained from TCGA. (*O*) Kaplan–Meier plot showing that high copy number of the PRL gene correlates with low survival in patients with cancer from the TCGA Pan-cancer (PanCan) cohort ($P < .0001$). (*P*) PRL mRNA levels are up-regulated across primary pancreatic adenocarcinomas ($n = 145$) compared with normal pancreatic tissue ($n = 46$), as previously reported from microarray expression data downloaded from the Gene Expression Omnibus (accession number: GSE71729) ($P = .0042$). (*Q*) Immunohistochemistry was used to evaluate PRL expression in PDAC TMA. Only β cells express high PRL levels in normal pancreas. However, in tumors, PDAC cells show high expression of PRLR. (*R*) Western blot analysis shows that PRL levels are higher in pancreatic cancer cell lines. (*S*) Differential expression of DRD2 mRNA in the various normal tissues adapted from the GTEx data set. RNA-sequencing data are reported as median RPKM, generated by the GTEx project. (*T*) DRD2 RNA-sequencing data in cancer types are reported as median FPKM, generated from data obtained from TCGA. (*U*) DRD2 mRNA levels are significantly high in PDAC cancer ($P < .01$) in the TCGA database. (*V*) Kaplan–Meier plot shows that high gene expression of the DRD2 gene correlates with low survival in with cancer from the TCGA Pan-cancer (PanCan) cohort ($P = .912$). (*W*) Immunohistochemistry to evaluate DRD2 expression in pancreatic tumor microarray from the University of Kansas Cancer Center. Pancreatic tumors show high levels of DRD2 expression, whereas expression in normal pancreas is low. Again, pancreatic β cells express high DRD2 levels in normal pancreas. (*X*) Immunohistochemistry: composite score shows significantly high expression of DRD2 in tumor compared with normal pancreas. (*Y*) Composite score of immunohistochemistry shows significantly higher expression of DRD2 in various types of PDAC compared with normal pancreas.

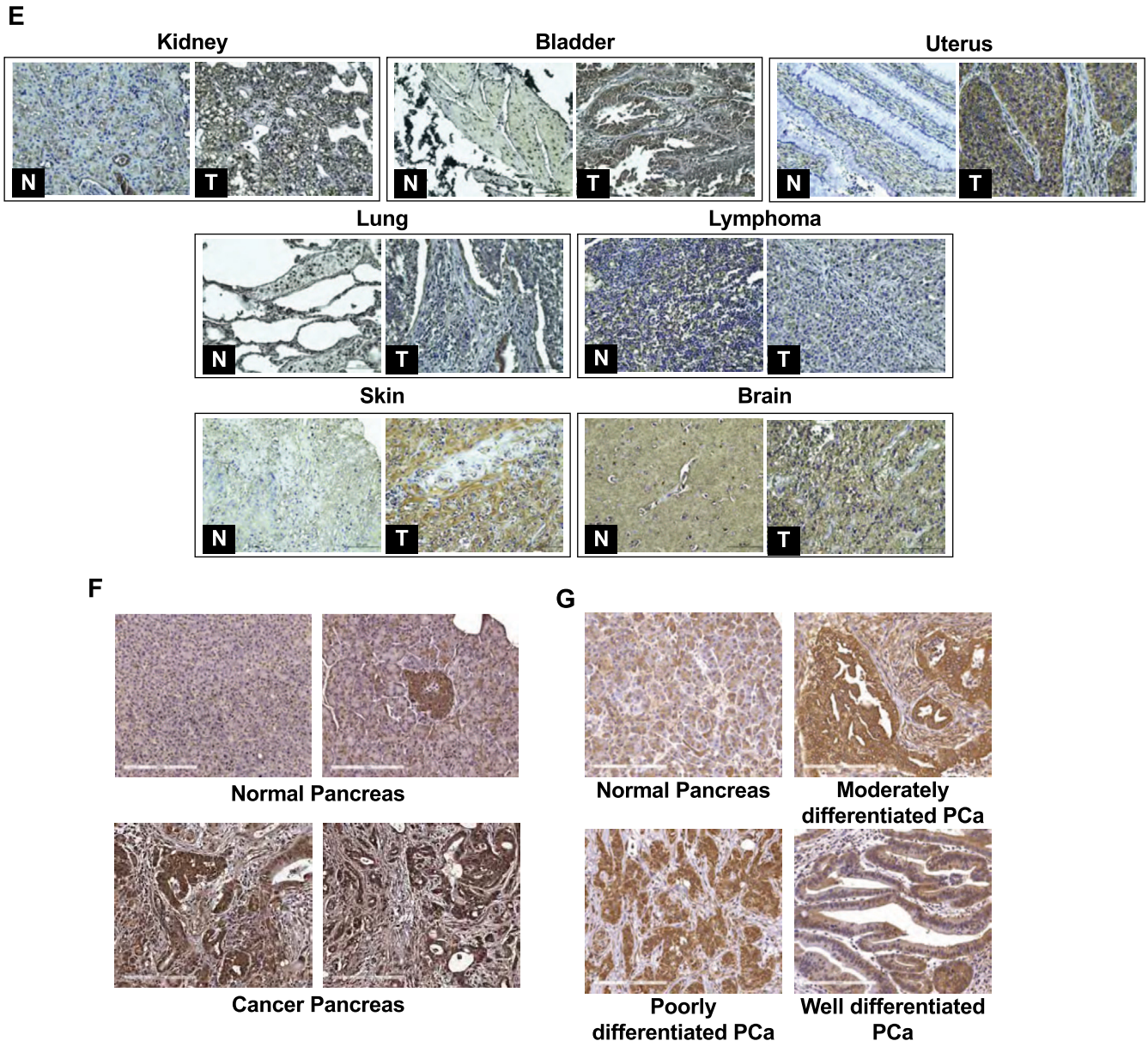

Supplementary Figure 1. (*continued*).

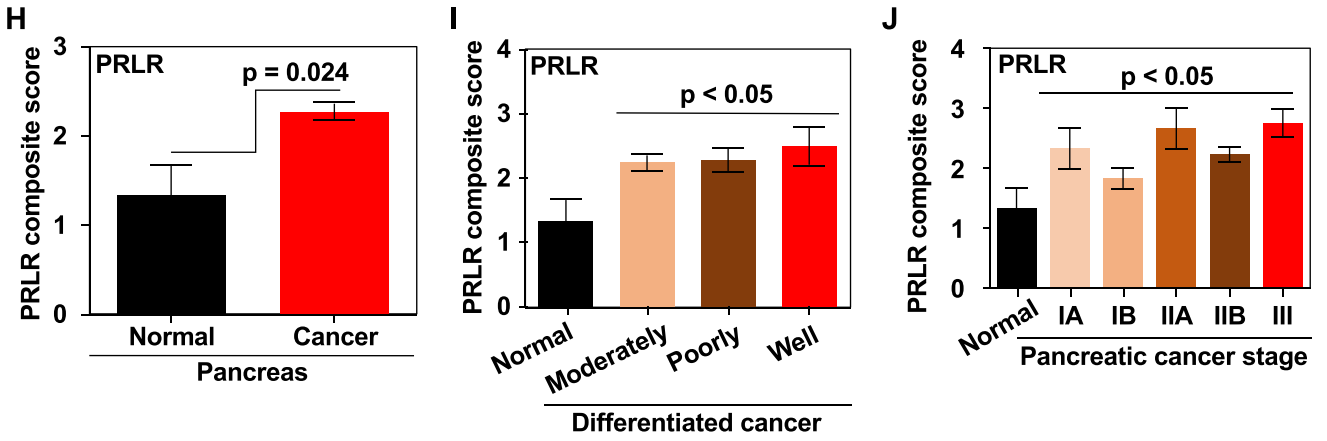

K

Parameter	Sub-parameter	Average score	p value
Sex	Male	2.2	0.928
	Female	2.3	
Age	< 60	2.4	0.110
	> 60	2.1	
LVI	Absent	2.3	0.622
	Present	2.4	
PNI	Absent	2.0	0.607
	Present	2.3	
Tumor size	< 2	2.2	0.919
	> 2	2.2	

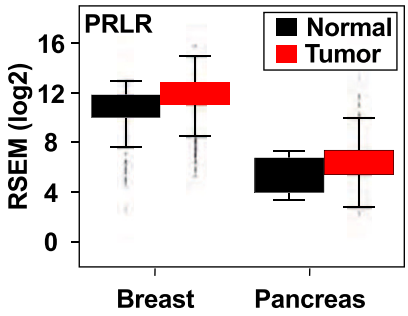

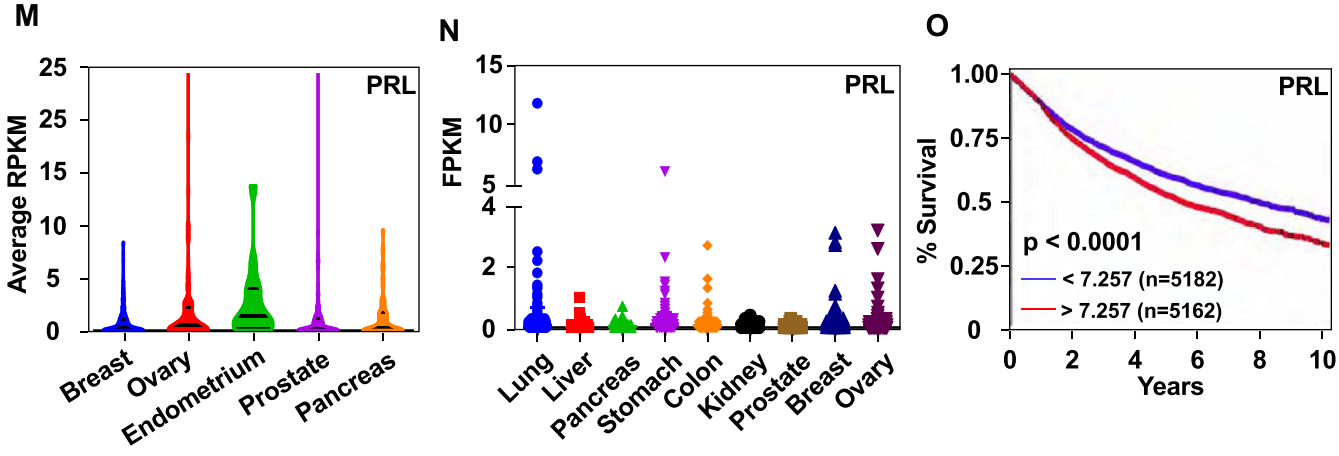

Supplementary Figure 1. (*continued*).

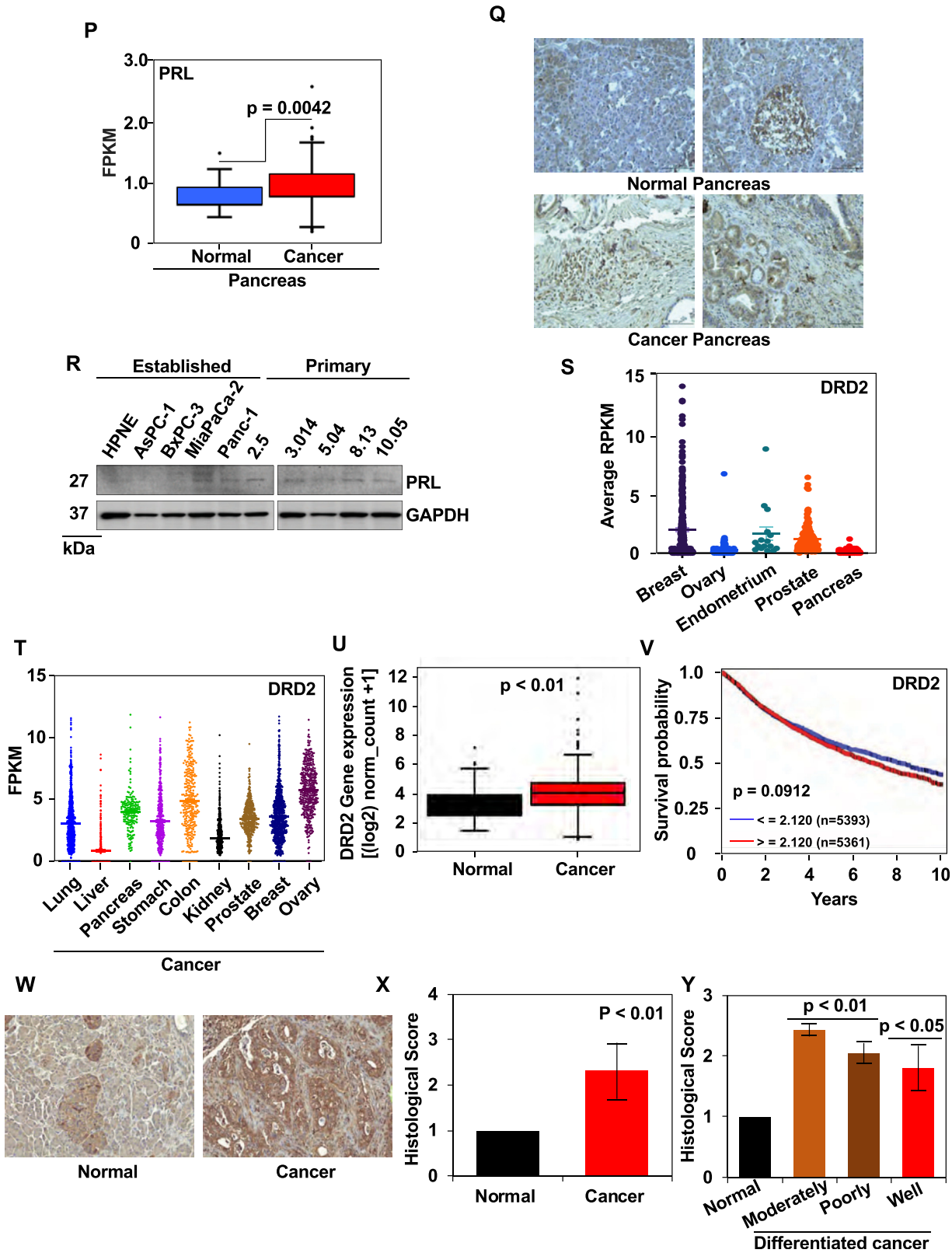

Supplementary Figure 1. (*continued*).

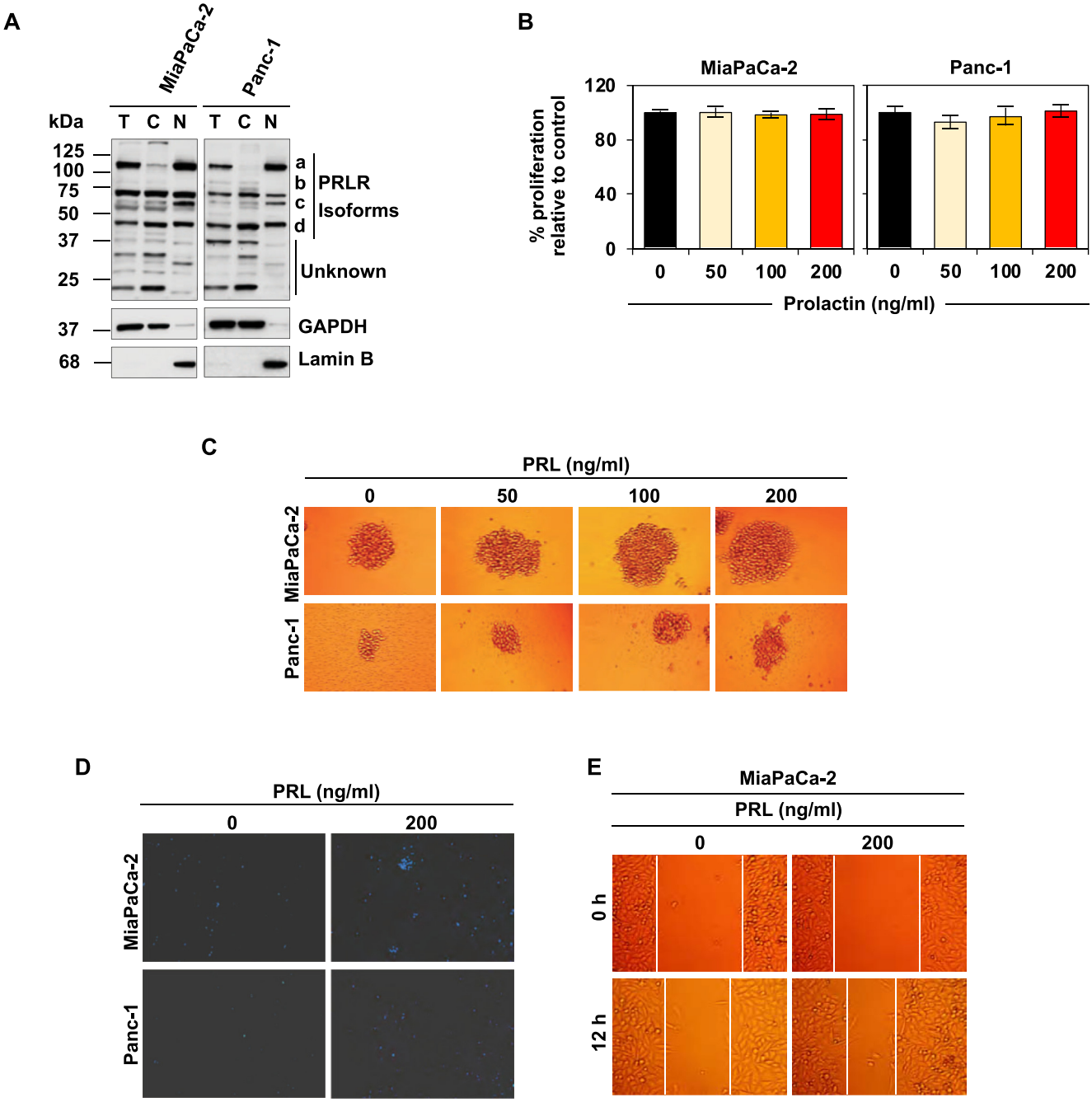

Supplementary Figure 2. (*A*) Western blot analysis shows that PRLR is present in both nuclear and cytoplasmic fraction in Panc-1 and MiaPaCa-1 PDAC cell lines. Glyceraldehyde-3-phosphate dehydrogenase (GAPDH) and Lamin B were used as internal controls for cytoplasmic and nuclear extracts, respectively. (*B*) PRL treatment at increasing doses (50–200 ng/mL) does not affect proliferation of PDAC cells for up to 72 hours. (*C*) PRL affects pancosphere formation. PDAC cells were grown in specific spheroid media in ultra-low-binding plates and treated with increasing doses of PRL (0–200 ng/mL). The pancospheres were photographed and counted after 10 days. A significant increase in spheroid size was observed in the presence of PRL. (*D*) PRL affects transwell migration. PRL (200 ng/mL) treatment induces migration in MiaPaCa-2 and Panc-1 cell lines over a period of 12 hours in a transwell/Boyden chamber assay. After 12 hours, cells fixed with formalin, stained with 4′,6-diamidino-2-phenylindole and imaged with a fluorescence microscope. (*E*) PRL affects scratch plate migration. PRL (200 ng/m:) treatment induces migration in MiaPaCa-2 cell lines over a period of 12 hours in scratch plate assay, photographed with a light microscope. h, hour.

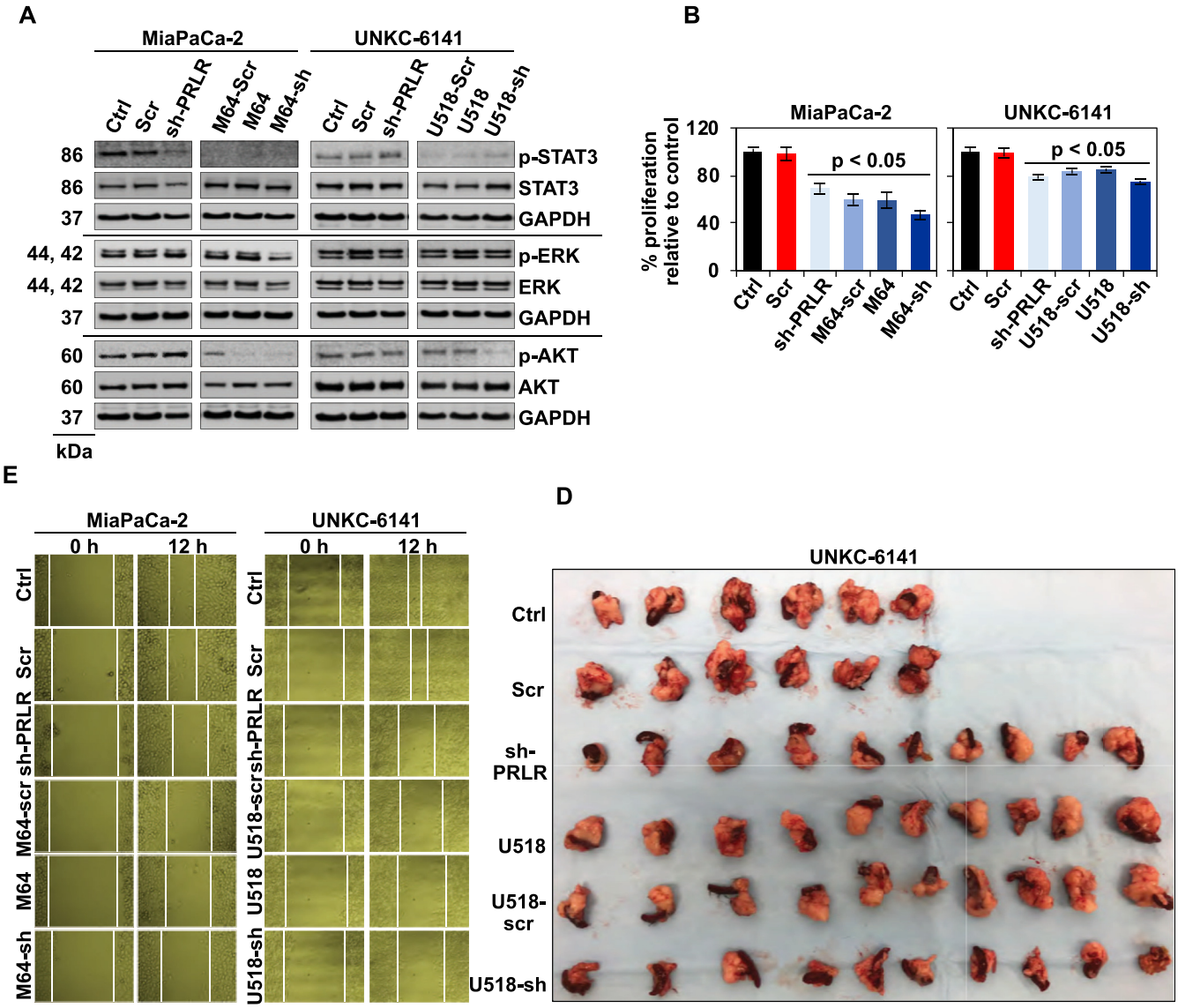

Supplementary Figure 3. (*A*) Western blot analyses show that suppressing PRLR expression leads to reduced phosphorylation of ERK, STAT3, and AKT in MiaPaCa-2 and UNKC-6141 PDAC cells where PRLR is knocked down. M64 and U518 are clustered regularly interspaces short palindromic repeats (CRISPR)/Cas9 PRLR knockdown clone of MiaPaCa-2 and UNKC-6141 cells, respectively. Scr, scrambled shRNA; sh-PRLR: PRLR-specific shRNA. (*B*) MiaPaCa-2 and UNKC-6141 cells lacking PRLR exhibited lower rates of proliferation compared with their respective control cells ($P < .05$). (*C*) Cells lacking PRLR showed reduced ability to migrate in the scratch plate assay compared with their respective control cells. (*D*) UNKC6141 cells with shRNA alone (control (Ctrl], Scr, sh-PRLR) or after CRISPR (U518, U518-Scr, U518-Sh) were injected into the pancreas of C57BL/6 mice, and tumors were allowed to develop for 28 days. On day 29, tumors were excised and subjected to further analyses. All of the PRLR-knockdown cells (sh-PRLR, U518, U518-scr, U518-sh) developed smaller tumors compared with the control group. (*E*) Immunohistochemistry analyses of PRLR down-regulated U518-sh tumors showed a lower number of proliferating cell nuclear antigen (PCNA)–positive nuclei than control tumors ($P < .01$). (*F*) Quantification of the number of PCNA-positive cells showed reduced numbers of PCNA-positive nuclei in U518-sh cells compared with controls. (G) The excised PDAC orthotopic tumors were cut into small parts, homogenized in lysis buffer, sonicated, and subjected to Western blot analyses. PRLR–down-regulated U518-sh-PRLR tumors showed reduced levels of ERK, STAT3, and AKT phosphorylation compared with controls.

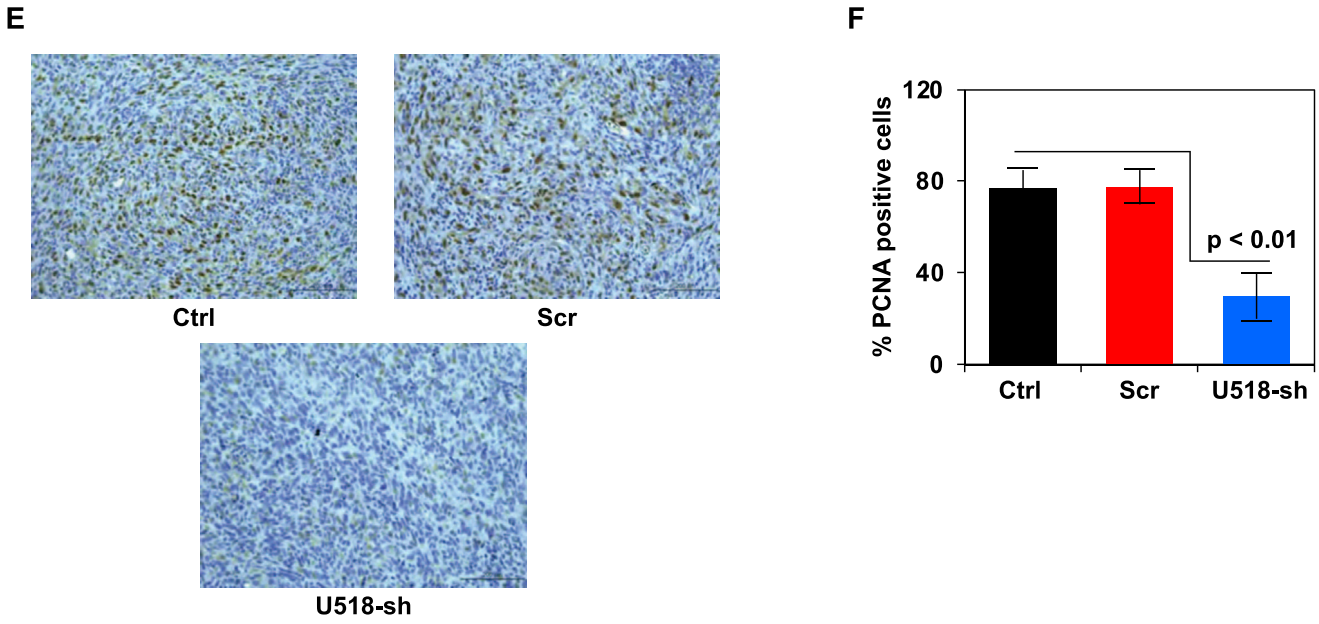

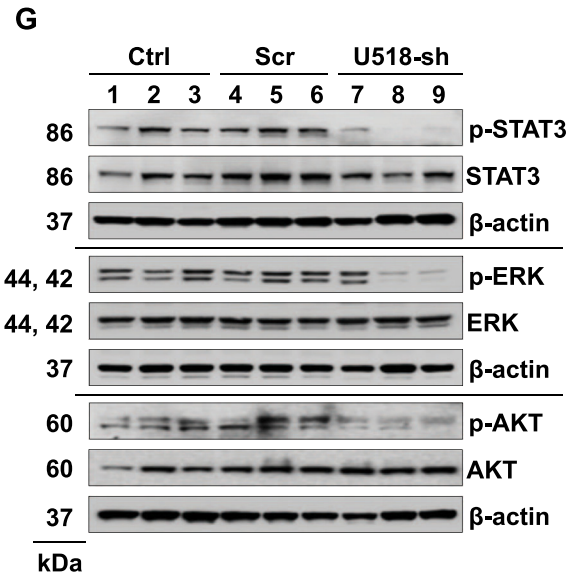

Supplementary Figure 3. (*continued*).

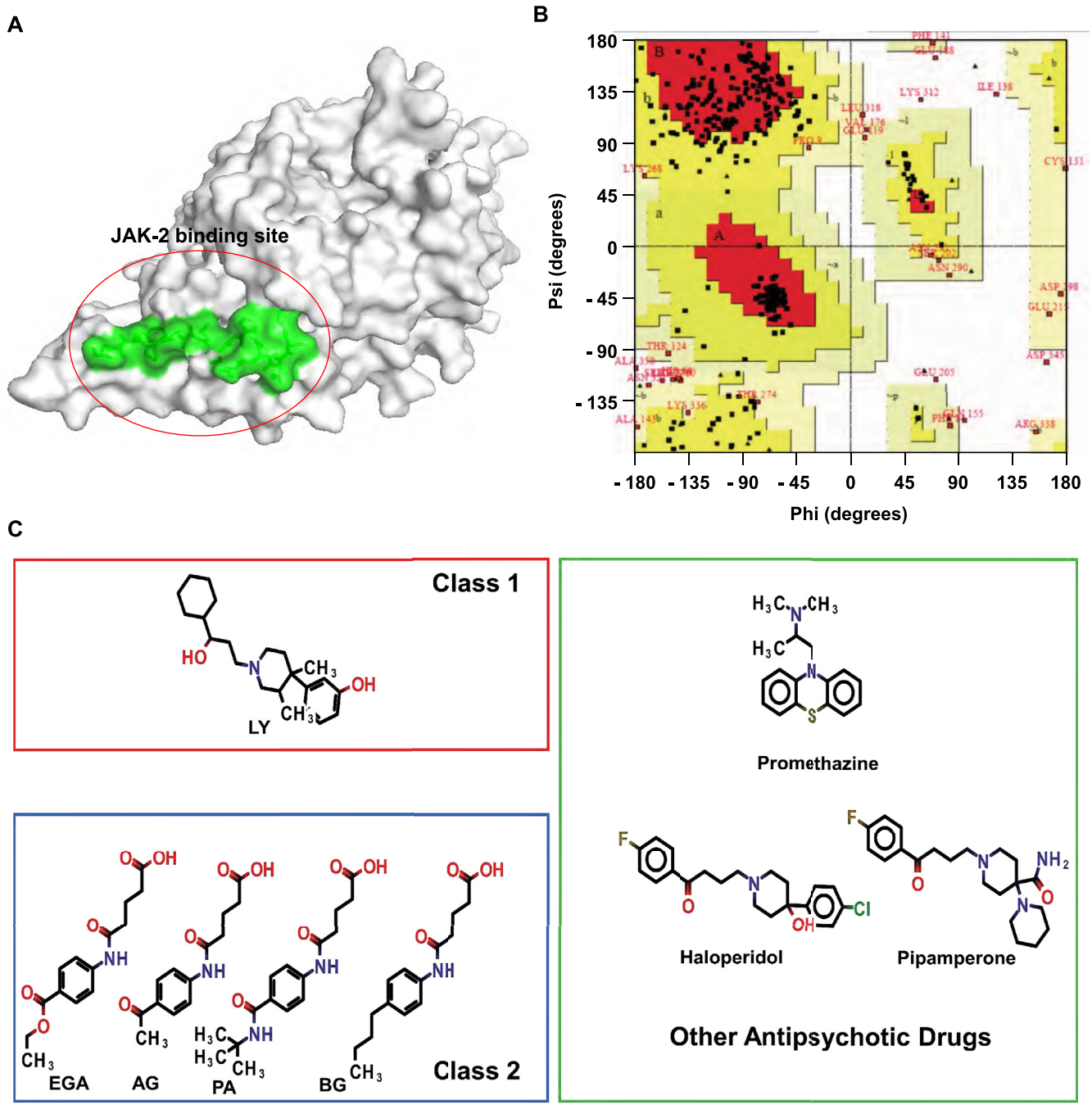

Supplementary Figure 4. (*A*) Homology modeling. The Phyre2 online server (http://www.sbg.bio.ic.ac.uk/phyre2/html/page.cgi?id=index) was used to generate the protein structure of the cytoplasmic domain of PRLR. The JAK2 binding site is shown in green. (*B*) The predicted homology model is characterized by Ramachandran plot (http://www.ebi.ac.uk/thornton-srv/databases/pdbsum/Generate.html). (*C*) The fragment-based drug discovery approach was used to identify structurally similar compounds, as indicated in red boxes in panel *A*. Six compounds were identified initially, and penfluridol, a known antipsychotic drug, was found to bind the receptor as well as inhibit proliferation in PDAC cells. Furthermore, 6 drugs belonging to 3 different chemical class of antipsychotic drugs were identified such as butyrophenones (haloperidol and pipamperone), diphenylbutylpiperidines (fluspirilene and pimozide) and phenothiazines (promethazine and fluphenazine). (*D, E*) Molecular docking. AutoDock Vina software (http://vina.scripps.edu/) was used to perform docking of selected compounds into PRLR protein cavity. JAK2 binding site (*green*) was used to design the grid. The best stable conformation is presented (*yellow*, interacting residues; *pink*, compound). (*F*) Molecular docking. The table shows molecular docking interactions and consequence scores of best conformations of compound–PRLR binding. (*G*) Antiproliferative activity in MiaPaCa-2 and Panc-1 cells. Cells were incubated with increasing doses (0–40 μmol/L) of LY255582 (LY), 4-acetylglutaranilic acid (AG), 5-{4-[(tert-Butylamino)carbonyl]anilino}-5-oxopentanoic acid (PA), 4-(ethoxycarbonyl)-glutaranilic acid (EGA), and 4-butylglutaranilic acid (BG) for up to 72 hours and analyzed for cell proliferation. None of these compounds inhibits proliferation. (*H*) Antiproliferative activity in MiaPaCa-2 and Panc-1 cells. Cells were incubated with increasing doses (0–40 μmol/L) of haloperidol, promethazine, and pipamperone for up to 72 hours and analyzed for cell proliferation. These compounds inhibit proliferation at higher doses. (*I*) Penfluridol inhibits proliferation of pancreatic cancer cells. Cells were incubated with increasing doses of penfluridol (0–40 μmol/L) for up to 72 hours and analyzed for cell proliferation. Penfluridol treatment suppressed PDAC cell proliferation in all cell lines when compared with untreated controls in a dose- and time-dependent manner. (*J*) The half maximal inhibitory concentration (IC_{50}) values for antiproliferative effects of antipsychotics are summarized in the table. (*K*) The IC_{50} values for the antiproliferative effects of penfluridol against PDAC cell lines are summarized in the table. (*L*) Fluphenazine, fluspirilene, pimozide (10 μmol/L) and promethazine (30 μmol/L) inhibit colony formation. Pancreatic cancer cell lines were incubated with compounds for 48 hours and allowed to grow into colonies for 10 days. Incubation with these compounds inhibits colony formation at higher concentrations only. (*M*) Penfluridol inhibits colony formation. Pancreatic cancer cell lines were incubated with 4 μmol/L penfluridol for 48 hours and allowed to grow into colonies for 10 days. Incubation with penfluridol inhibits colony formation. (*N*) Spheroid formation assay. MiaPaCa-2 and PanC-1 cells were grown in specific spheroid media in low-adherent plates and treated with increasing concentrations of compounds (AG, PA, EGA, and BG, 2–8 μmol/L). After 5 days, the pancosphere were photographed and counted. The compounds did not affect spheroid formation. (*O*) None of the compounds affected the number of spheroids. (*P*) Penfluridol (4 μmol/L) inhibits proliferation of PDAC cell lines MiaPaCa-2 and Panc-1 in the presence of PRL (200 ng/mL) over a period of 48 hours ($P < .01$). (*Q*) Antipsychotic drugs induce autophagy. Lysates from MiaPaCa-2 or Panc-1 cells incubated with fluphenazine, fluspirilene, pimozide, and promethazine (IC_{50} value) were analyzed by Western blotting for LC3B and p62. (*R*) Caspase-3/7 assay: MiaPaCa-2 and Panc-1 cells were treated with PEN (2–8 μmol/L) over a period of 48 hours. Commercial caspase-3/7 assay kit was used to estimate activity. Penfluridol induced caspase-3/7 activation at 48 hours at 8-μmol/L concentration ($P < .001$), whereas lower concentrations were unable to induce caspase-3/7 activation. (*S*) Penfluridol (0–5 μmol/L) did not inhibit proliferation of PDAC cell lines MiaPaCa-2 and UNKC-6141 when PRLR was knocked down to the same levels as their PRLR-sufficient respective controls (Ctrl). M64 and U518 are CRISPR/Cas9 clones knocking down PRLR from MiaPaCa-2 and UNKC-6141 cells, respectively. Scrambled shRNA (Scr), sh-PRLR, and PRLR-specific shRNA. (*T*) IC_{50} values. Penfluridol did not inhibit proliferation of PDAC cell lines MiaPaCa-2 and UNKC-6141 lacking PRLR to the same level as their PRLR-sufficient respective controls. (*U*) Penfluridol and gemcitabine combination inhibits proliferation of pancreatic cancer cells. Cells were incubated with increasing doses of a combination of penfluridol (PEN, 0–20 μmol/L) with gemcitabine (0–10 μmol/L) for up to 72 hours and analyzed for cell proliferation. Penfluridol and gemcitabine combination treatment suppressed PDAC cell proliferation in all cell lines compared with untreated controls in a dose- and time-dependent manner. (*V*) Penfluridol (PEN) and gemcitabine (GEM) produce synergistic activity in PDAC cell lines. Combinatorial index (CI) values are as follows: synergism (S), CI of 0.3–0.7; moderate synergism (MS), CI of 0.7–0.85; slight synergism (SS), CI of 0.85–0.9 (*W*) The normalized isobolograms showing for combination of penfluridol and gemcitabine in PDAC cells. M, mol/L.

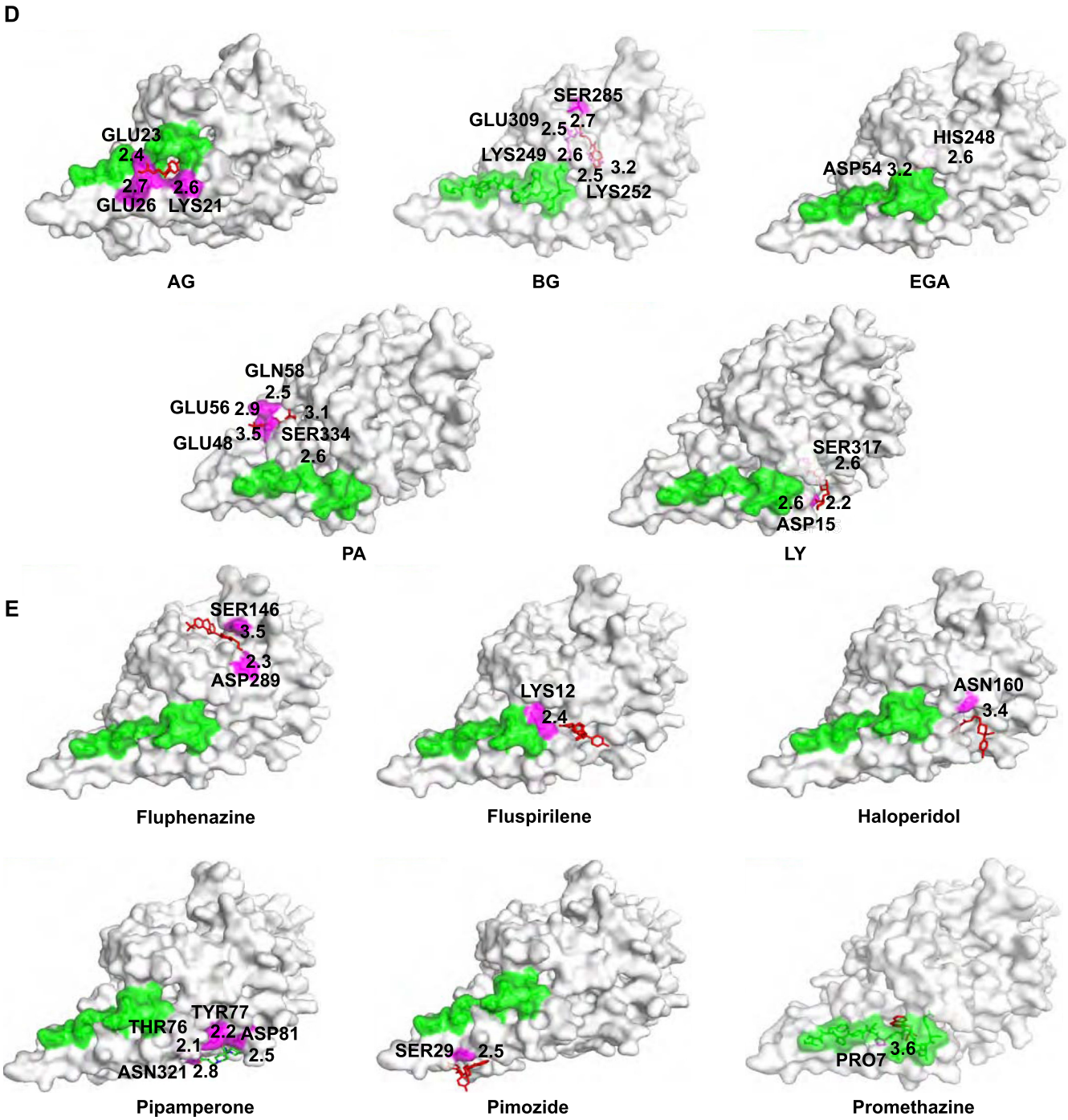

Supplementary Figure 4. (*continued*).

F

Compound	B.E. (Kcal/mol)	No of H bonds	Amino acid residue	Bond length (Å)
PEN	- 7.2	1	PRO7	1.9
LY	- 6.8	3	ASP15	2.6
			SER317	2.6 & 2.2
BG	- 6.7	5	SER285	2.7
			GLU309	2.5
			LYS249	2.6
			LYS252	2.5 & 3.2
AG	- 5.7	3	GLU23	2.4
			GLU26	2.7
			LYS21	2.6
EGA	- 4.9	2	ASP54	3.2
			HIS248	2.6
PA	- 5.6	5	GLN58	2.5
			GLU56	2.9
			GLU48	3.5
			SER334	2.6 & 3.1
Pimozide	-6.5	1	SER29	2.5
Fluspirilene	-7.2	1	LYS12	2.4
Fluphenazine	-6.8	2	SER146	3.5
			ASP289	2.3
Promethazine	-5.9	1	PRO7	3.6
Haloperidol	-7.0	1	ASN160	3.4
Pipamperone	-5.9	4	TYR77	2.2
			THR76	2.1
			ASN321	2.8
			ASP81	2.5

G

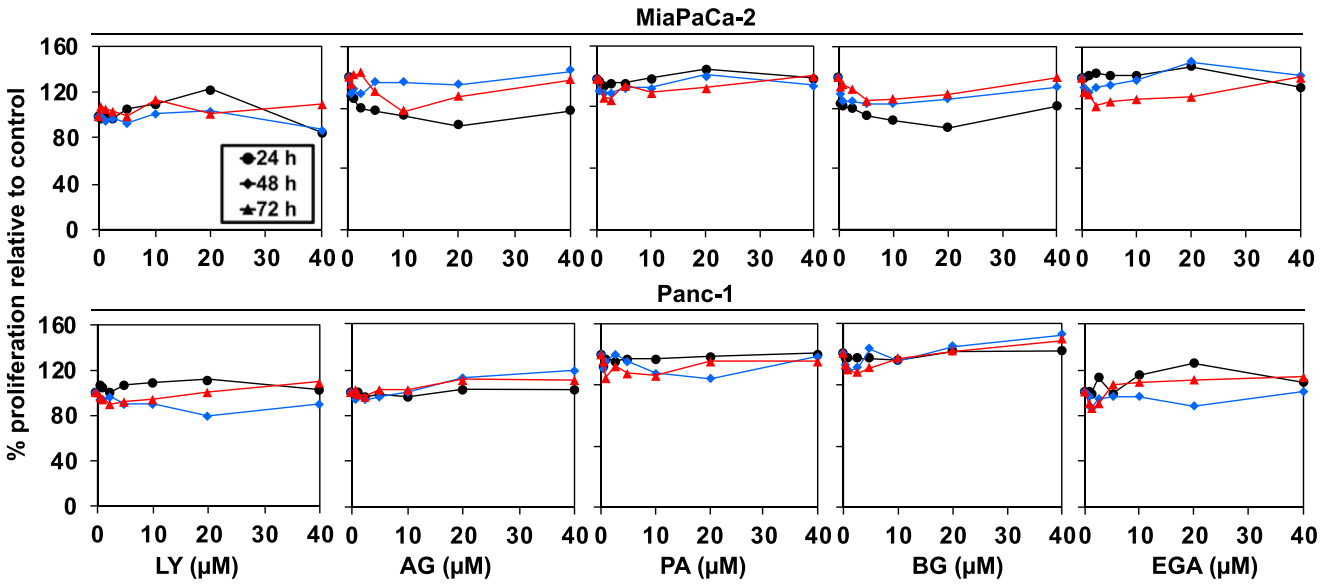

Supplementary Figure 4. (*continued*).

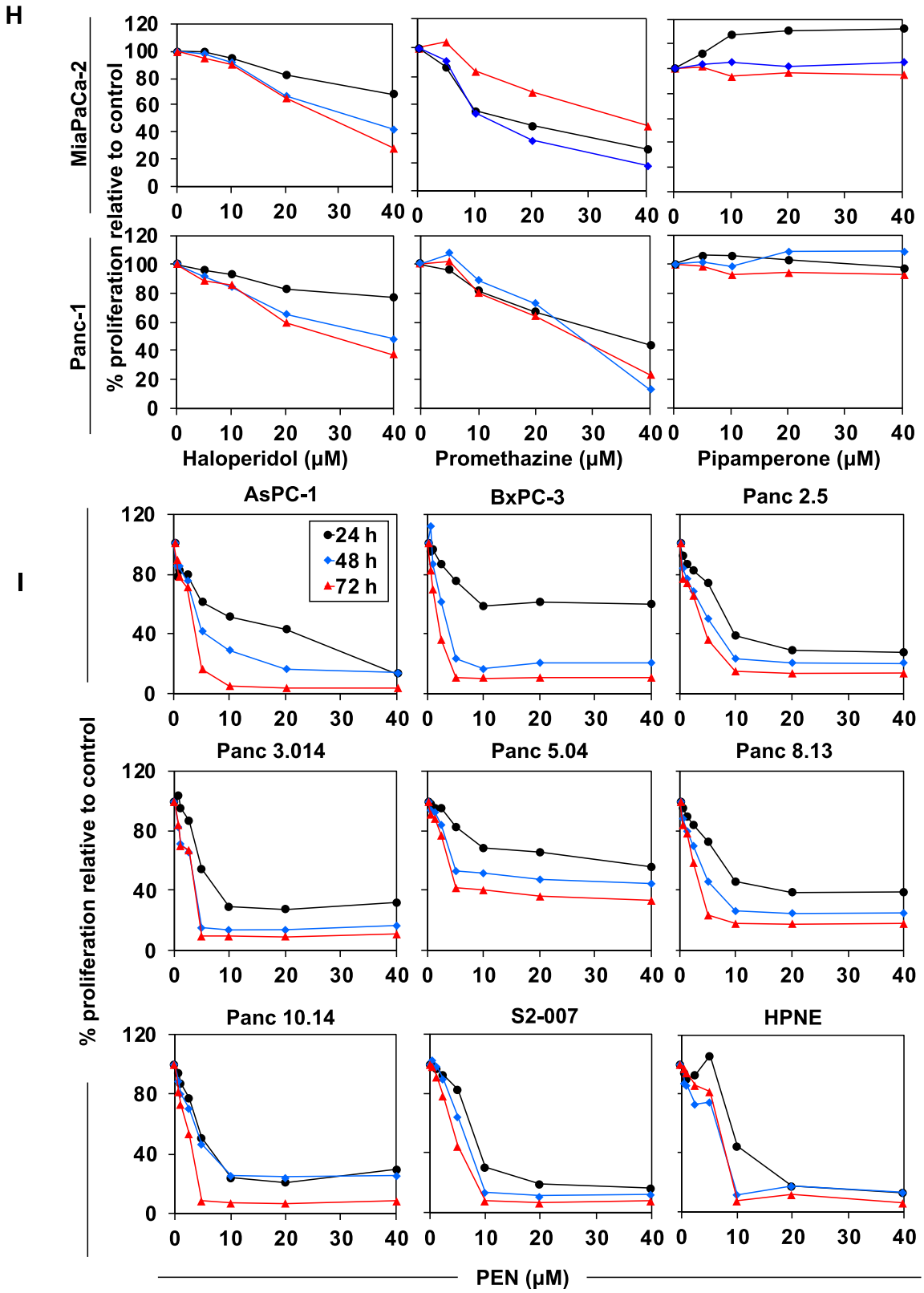

Supplementary Figure 4. (*continued*).

J

Drugs	MiaPaCa-2			Panc-1		
IC50 values	24 h	48 h	72 h	24 h	48 h	72 h
Pimozide	12	9	7.5	23	10	8
Fluspirilene	18	14	12	25	12	10
Fluphenazine	12	9	8	20	10	7
Promethazine	38	18	12	35	28	27
Haloperidol	>40	37	29	>40	40	30
Pipamperone	>40	>40	>40	>40	>40	>40

K

Cell lines	IC_{50} value (μM)		
	24 h	48 h	72 h
AsPC-1	10.0	4.1	3.2
BxPC-3	5.2	2.0	2.2
Panc-1	6.5	4.0	3.1
MiaPaCa-2	4.2	3.0	3.0
Panc 2.5	8.5	5.1	3.7
Panc 3.014	5.1	3.2	3.2
Panc 5.04	> 40	12.0	4.4
Panc 8.13	9.0	5.4	3.4
Panc 10.14	4.8	3.2	2.8
S2-007	8.2	6.5	4.5
HPNE	9.1	6.8	6.7

L

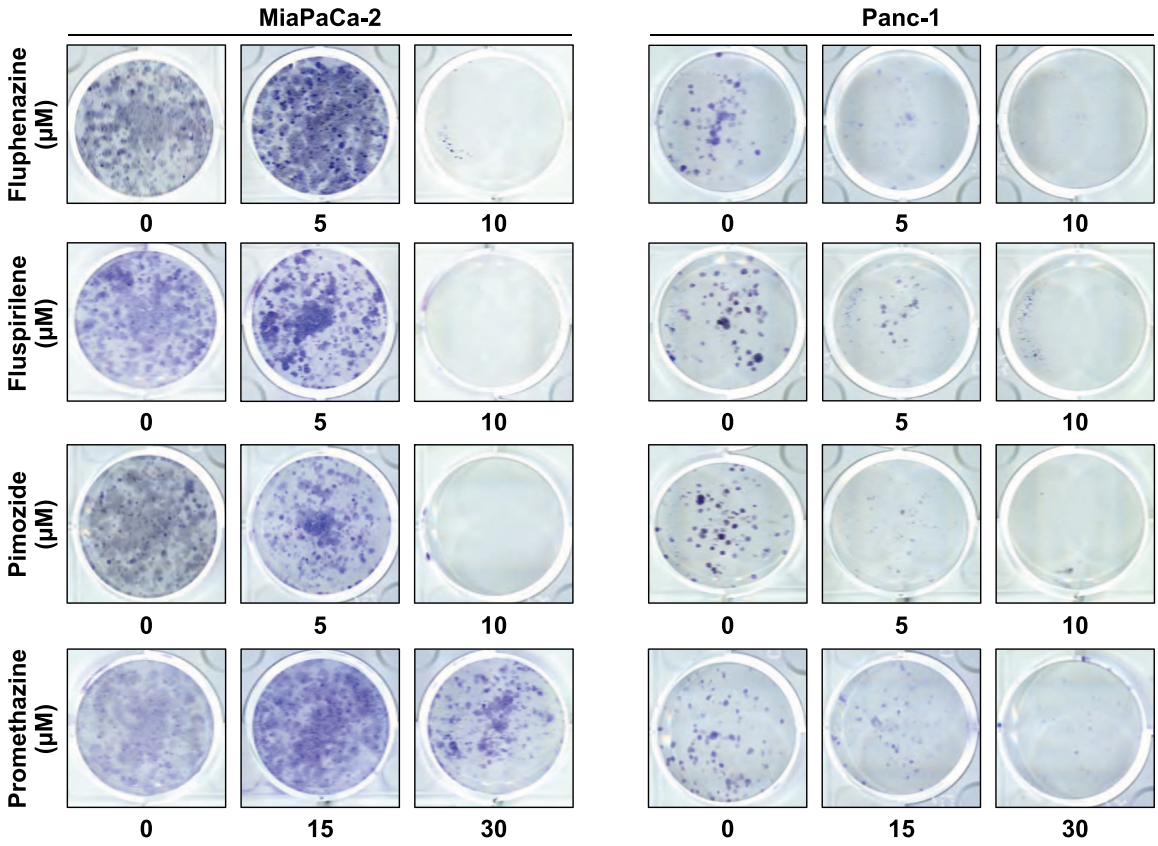

Supplementary Figure 4. (*continued*).

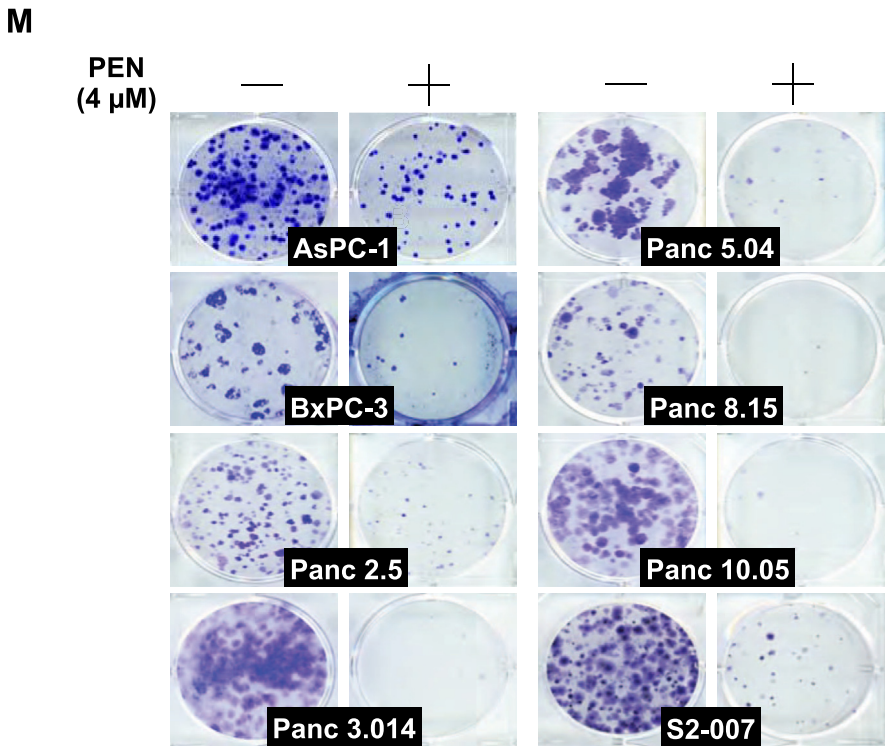

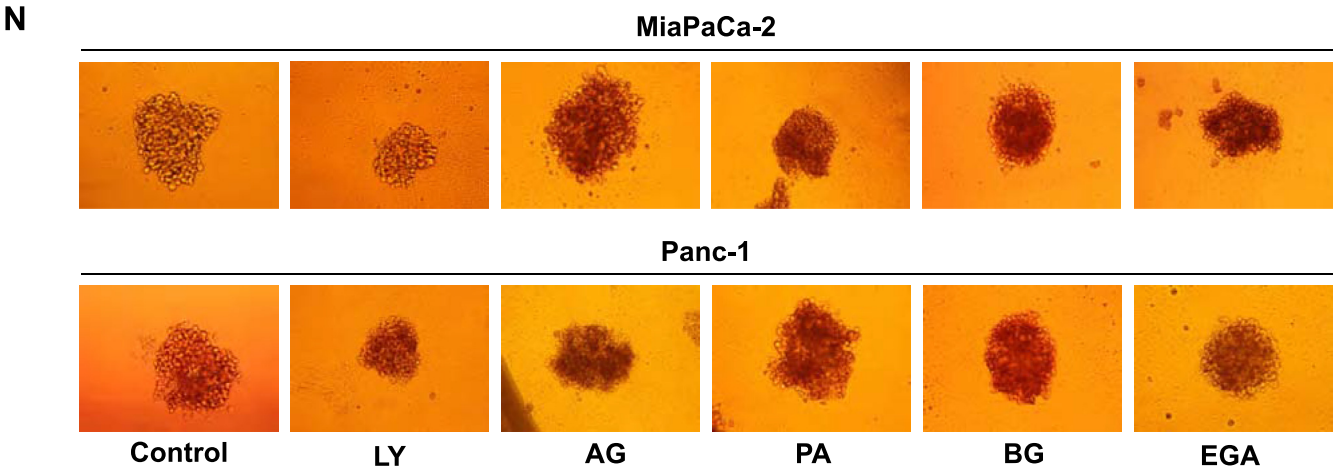

Supplementary Figure 4. (*continued*).

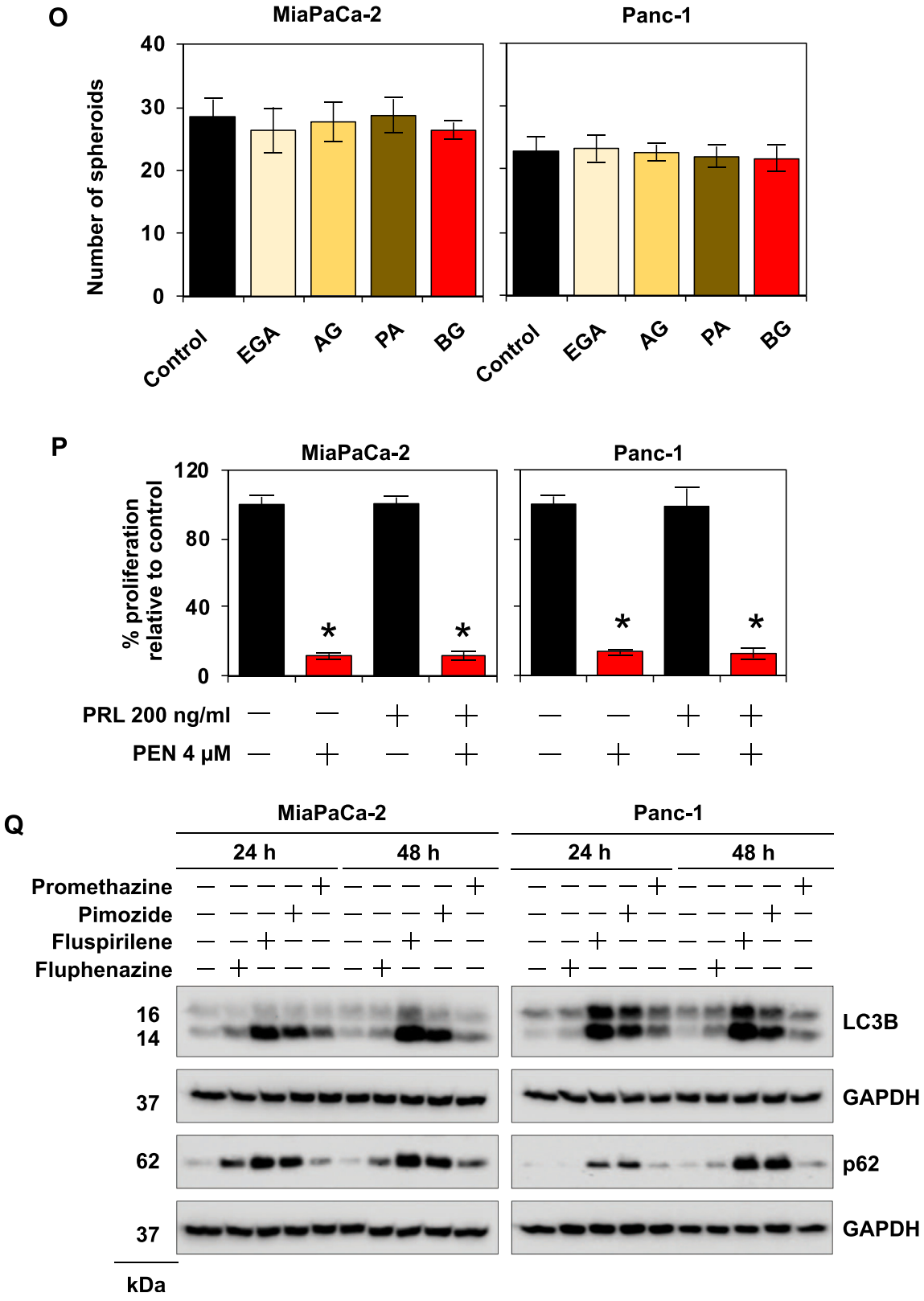

Supplementary Figure 4. (*continued*).

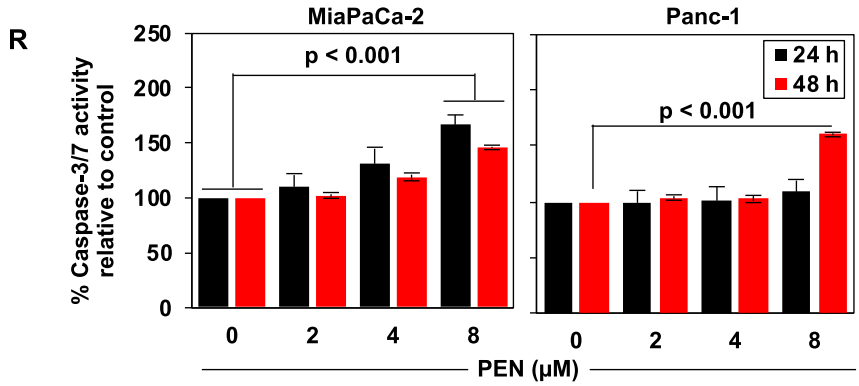

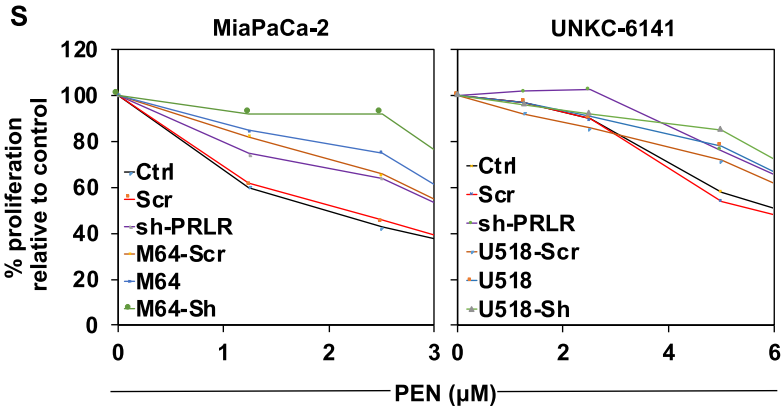

T

MiaPaCa-2 (IC_{50} value)		UNKC-6141 (IC_{50} value)	
Ctrl	2.0	Ctrl	5.8
Scr	2.1	Scr	6.0
sh-PRLR	3.3	sh-PRLR	7.5
M64	3.4	U518	7.6
M64-scr	3.2	U518-scr	7.4
M64-sh	3.8	U518-sh	7.5

Supplementary Figure 4. (*continued*).

U

MiaPaCa-2

10 Gemcitabine (μM) 0						20 PEN (μM) 0
13.5	13.6	13.1	12.6	13.1	12.7	
11.4	11.4	11.4	11.3	11.6	11.4	
10.5	10.7	10.5	10.7	10.5	10.9	
25.5	24.9	29.2	40.8	41.1	42.5	
35.7	35.6	46.8	57.8	61.5	64.7	
39.8	41.7	48.9	65.1	69.1	71.2	
41.7	44.1	57.0	71.1	78.3	81.4	
48.2	48.6	60.9	81.3	93.3	100.0	

Panc-1

10 Gemcitabine (μM) 0						10 PEN (μM) 0
8.1	8.3	8.0	8.0	8.2	8.4	8.4
15.2	16.3	18.2	22.7	23.2	26.7	23.8
29.6	34.0	42.1	54.3	59.5	63.6	71.4
31.5	35.7	47.2	59.9	63.9	68.3	75.7
33.2	35.5	48.3	62.1	64.4	69.2	78.6
35.5	36.6	50.1	61.5	64.7	74.2	88.3
39.3	41.9	58.7	73.8	75.1	82.5	89.2
42.5	44.1	53.6	78.3	86.7	87.8	100.0

V

MiaPaCa-2		
PEN (μM)	GEM (μM)	CI
2.5	10.0	0.73 MS
2.5	5.0	0.53 S
2.5	2.5	0.57 S
1.25	5.0	0.66 MS
1.25	2.5	0.94 SS
0.625	2.5	0.66 S

Panc-1		
PEN (μM)	GEM (μM)	CI
2.5	5.0	0.34 S
2.5	2.5	0.42 S
2.5	1.25	0.54 S
2.5	0.312	0.59 S
1.25	1.25	0.59 S
1.25	0.625	0.64 S
0.625	0.625	0.62 S
0.625	0.312	0.64 S

W

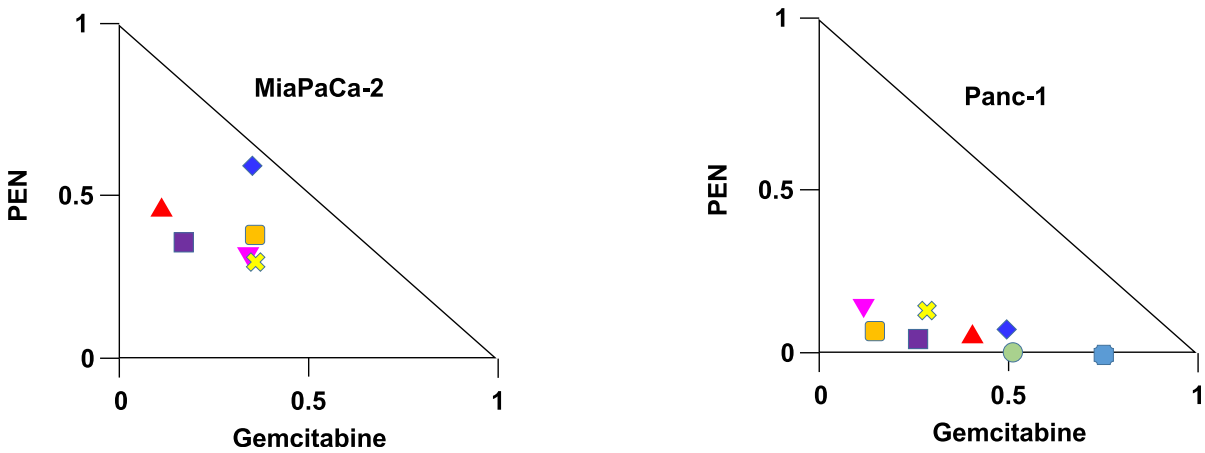

Supplementary Figure 4. (*continued*).

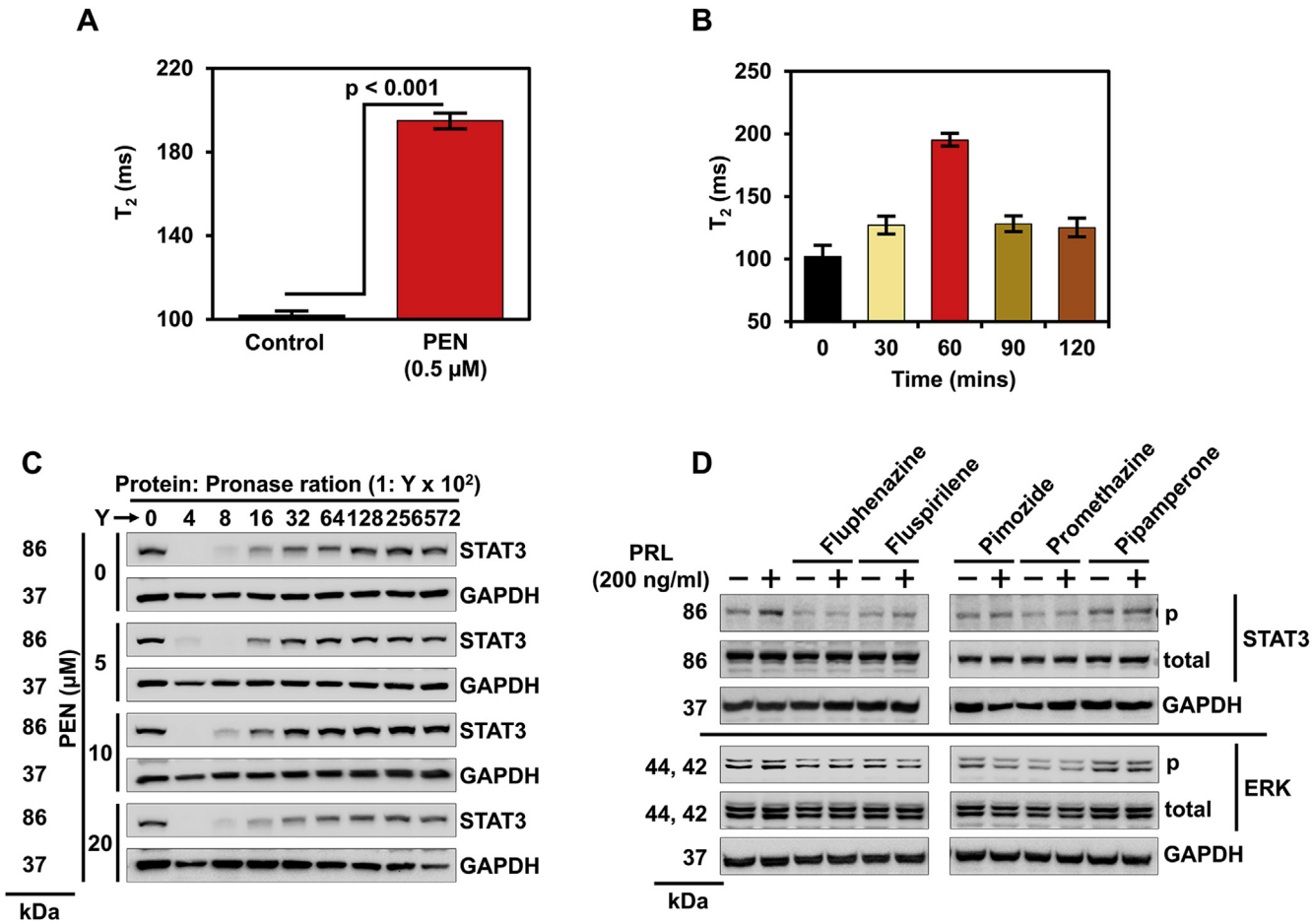

Supplementary Figure 5. (*A*) Magnetic relaxometric technique. Iron supermagnetic nanoparticles were synthesized and conjugated with JAK2 binding peptide. The nanoparticles were then incubated with penfluridol (500 nmol/L) *(P* < .001). Higher T2 values were recorded after compound binding to the peptide conjugate. (*B*) Penfluridol binds to the PRLR JAK2 binding site. Iron supermagnetic nanoparticles were synthesized and conjugated with JAK2 binding peptide and incubated with penfluridol (500 nmol/L). Maximum binding occurs at 1 hour, after which the binding reduces. (*C*) Drug affinity responsive target stability (DARTS). MiaPaCa-2 cells were treated with different concentrations of penfluridol (0–20 μmol/L) and subjected to lysis with different concentrations of pronase. Resulting lysates were subjected to Western blot analyses. Penfluridol protected PRLR against pronase-induced cell lysis, suggesting penfluridol–PRLR binding. STAT3 stability is not affected by PEN, suggesting lack of interaction of the protein with the compound. This also suggests specific binding of the compound to PRLR. (*D*) Antipsychotic drugs fluphenazine, fluspirilene, pimozide, and promethazine inhibits PRL-induced ERK and STAT3 phosphorylation. Cells were pretreated with antipsychotic drugs for 4 hours, followed by PRL for 30 minutes. Western blot analyses show reduced ERK and STAT3 phosphorylation in response to antipsychotic drugs.

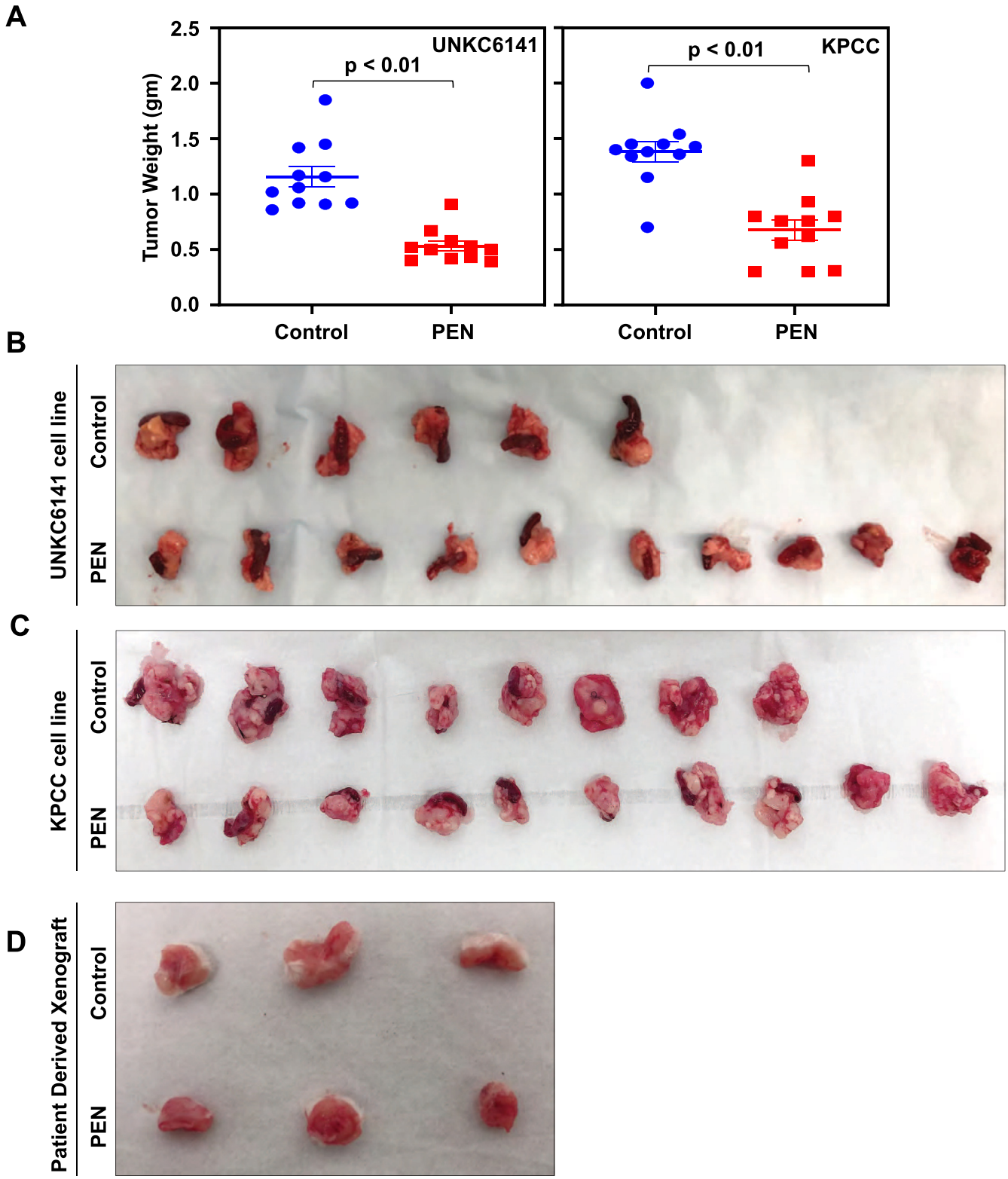

Supplementary Figure 6. (*A*) UNKC-6141 and KPCC cells were allowed to grow for 7 days and form tumors in the pancreas of C57BL/6 mice (n = 10). Subsequently, penfluridol (5 mg/kg of body weight) was injected intraperitoneally every day for 21 days. On day 29, tumors were excised and subject to further analyses. Penfluridol treatment resulted in significantly lower tumor weight when compared with control ($P < .01$). (*B*) Penfluridol (PEN) treatment significantly reduced the tumor size in UNKC-6141 cells. (*C*) Penfluridol treatment significantly reduced the tumor size in KPCC. (*D*) Penfluridol treatment resulted in significantly lower size compared with control in PDX tumor tissue. (*E*) Penfluridol treatment resulted in significantly ($P < .01$) smaller tumor size compared with control in Panc-1 xenograft tumors. (*F, G*) Immunohistochemistry analysis of penfluridol-treated tumors shows lower numbers of PCNA-positive nuclei than control tumors in C57BL/6 mice carrying orthotopic tumors of UNKC6141 and KPCC cells.

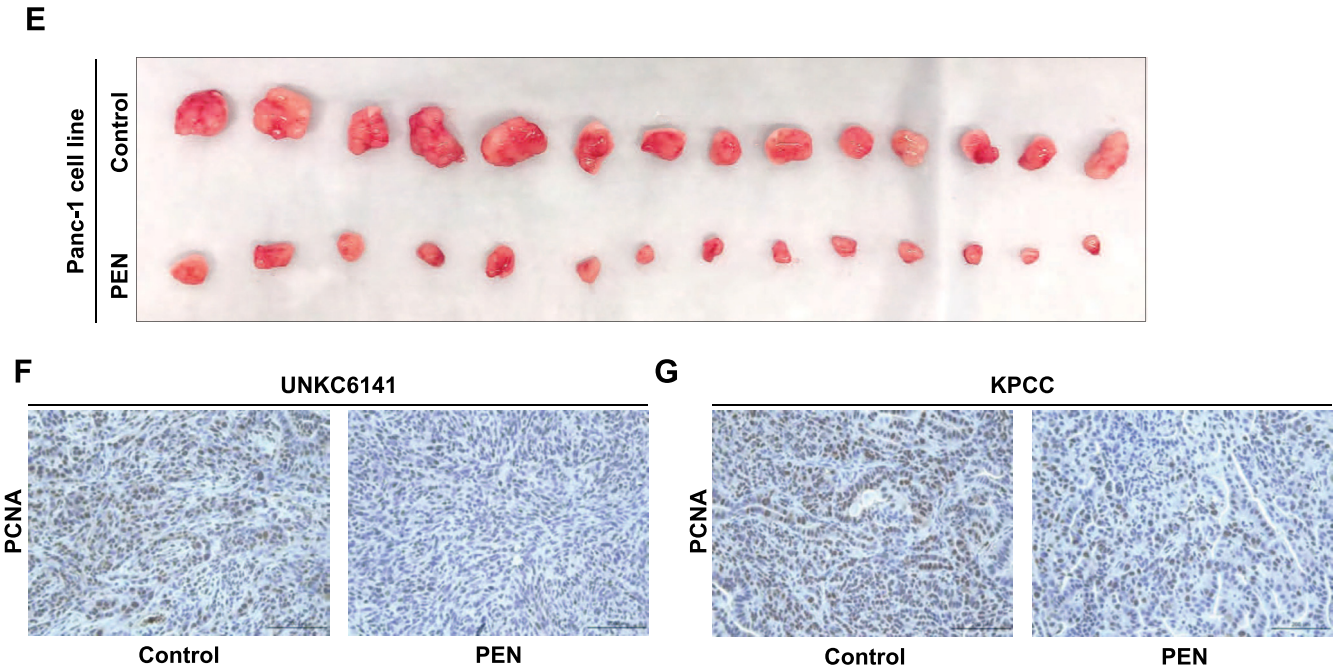

Supplementary Figure 6. (*continued*).

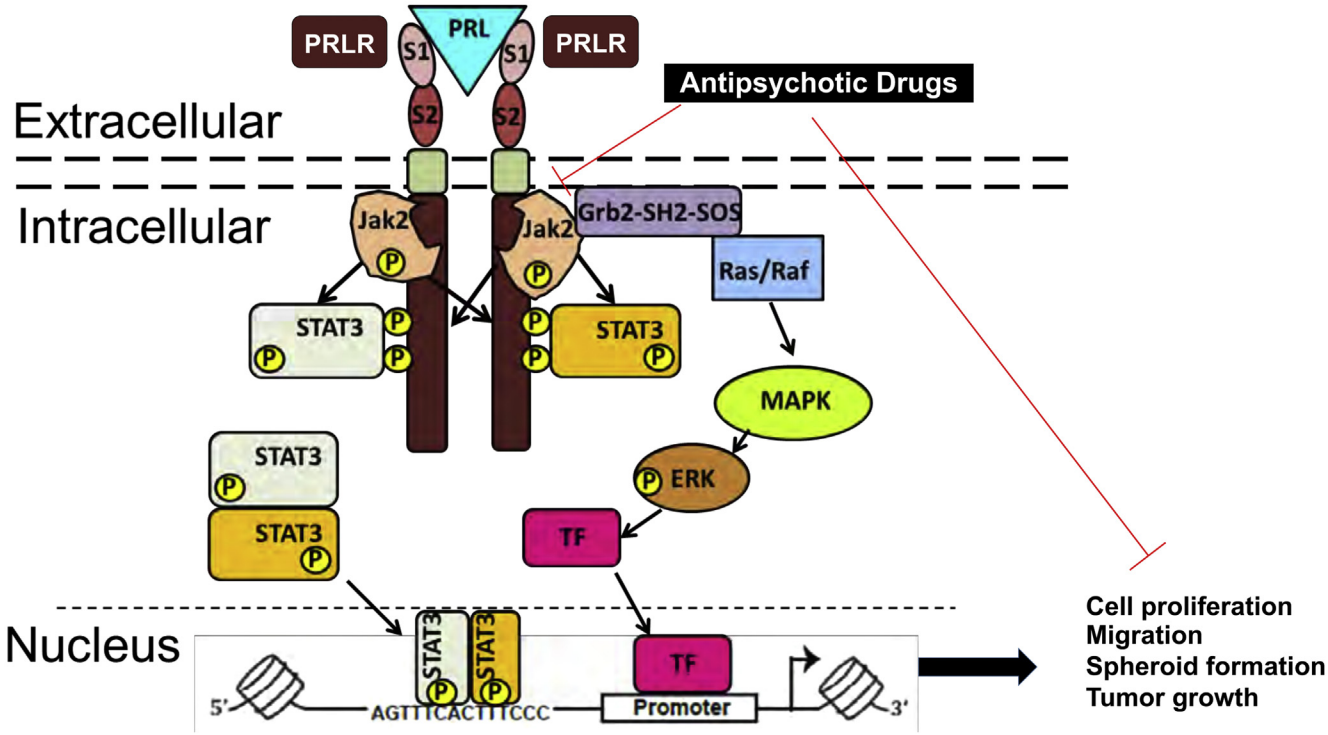

Supplementary Figure 7. Schematic representation of PRL–PRLR signaling and inhibition of tumor growth in PDAC.